Sandia National Laboratories

P.O. Box 5800
Albuquerque, New Mexico 87185-1137

June 17, 1998

Asimios Malliakos, Ph.D.
Accident Evaluation Branch
U.S. Nuclear Regulatory Commission
T-10-K-8
11545 Rockville Pike
Rockville, MD 20852

Subject: Results of the PP-1 and PP-2 PAR Experiments

Dear Dr. Malliakos:

The letter reports detailing the results and analysis of the PP-1 PAR experiment (to determine the PAR performance and flow) and the PP-2 PAR experiment (to determine the PAR hydrogen ignition criteria) are attached. SNL and NRC review comments on the draft reports were addressed in the final reports. I believe that the main objective, to determine the PAR performance, flow, and ignition criteria, has been satisfied. These technical reports are submitted as a required deliverable described in FIN JCN L2443.

I am also sending a copy of each report to Dieter Eder at NIS INGENIEURGESELLSCHAFT MBH and asking for a review concerning proprietary information. I will forward you his response when I receive it.

Note that each attachment contains two sets of text and one set of figures and pictures. Please replace the text in your draft reports (as the figures were not changed for the attached reports).

If you have questions, do not hesitate to call me.

Sincerely,

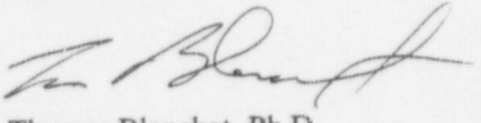

Thomas Blanchat, Ph.D.
Reactor Safety Experiments
Department 6423
Phone (505) 845-3048
FAX (505) 845-3435

Copies:
MS1139 K. O. Reil (6423)

Report on PAR Flow Measurements: The PP-1 Test

Background

The PP-1 PAR experiment performed in the Surtsey Test Facility was designed with two goals: 1) perform a counterpart experiment to PAR-9 or PAR-14 (Blanchat 1998) and look for similar behavior (i.e., a catalyst temperature spike at about 473 K suspected to be caused by the destruction of the hydrophobic coating) and 2) obtain PAR flow measurements at various hydrogen concentrations. Both goals required well-mixed conditions. On two separate occasions, flow measurements using an air/steam atmosphere were attempted. However, steam inside the vessel in conjunction with the extreme winter weather conditions caused numerous equipment and instrumentation problems, particularly in the operation of the x-y translator motors, the hot-wire anemometer, the pitot-tubes, and the mass spectrometer sampling system. Therefore, the flow measurement tests were performed in an air/hydrogen atmosphere.

Test Summary

The PAR was configured at 1/8 scale using new cartridges containing intact hydrophobic coating. The PAR was located at the centerline of the Surtsey vessel and about one meter above the false floor support I-beams. Pressure, temperature, and gas sampling instrumentation were as in previous tests (Blanchat 1998). The two pitot-tubes and the hot-wire anemometer were mounted on an x-y translator table that allowed a full traverse of the PAR at the chimney outlet (see attached pictures).

The Surtsey vessel was sealed and contained air at about 0.22 MPa. The initial gas temperature was about 286 K. First, the PAR was operated at a steady-state well-mixed condition by slowly injecting hydrogen and oxygen and continuously operating the mixing fans. The hydrogen flow rate (1 minute additions at 200 lpm for 15 s) was based on calculations showing that the average addition rate (about 50 lpm) was about equal to the scaled depletion rate at about 2 mole % hydrogen. The mixing fans were effective in maintaining a well-mixed condition inside the Surtsey vessel. The hydrogen concentration from the sample point located near the floor closely tracked the PAR inlet sample point.

At about t = 4.3 hours and at 1.6 mole % hydrogen, the catalyst temperature spiked upward and quickly returned to its previous value (about 460 K), replicating previous behavior (PAR-9 and PAR-14). The hydrogen concentration was then increased above 3.5 mole % to obtain flow data. Four sets of flow measurements were taken in well-mixed conditions:

1) at t = 5.535 hours and hydrogen concentration at 3.15 mole %,
2) at t = 6.025 hours and hydrogen concentration at 2.10 mole %,
3) at t = 6.480 hours and hydrogen concentration at 1.52 mole %,

4) at t = 7.510 hours and hydrogen concentration at 0.83 mole %.

Measured Data

Figures 1 and 2 show the temperatures recorded by the centerline (array A) and the near wall (array B) vertical vessel gas thermocouple arrays. The time of the mixing fan operation is given on the array B plot (Figure 2). From the start of the test until about 5.4 hours, hydrogen and oxygen was added into the Surtsey vessel simultaneously with operation of the mixing fans. Temperature stratification occurred rapidly when the fans were not operating, indicated by the separation of temperatures at the different heights on the thermocouple arrays. Figure 2 also plots the average of the array B temperatures; this average vessel temperature was used with an ideal gas law calculation to determine the moles of gas in the vessel.

Figures 3 and 4 show the cartridge catalyst and gap temperatures, respectively. Four specific points were instrumented: center of two middle cartridges (MIDCAR and MIDCAR BU), center of the wall cartridge (EDGCAR), and the corner of the same wall cartridge (CORCAR). The cartridge temperature (and corresponding gap) was measured near the bottom (location 1), in the middle (location 2) and near the top (location 3) along a vertical axis. The six middle cartridge thermocouples were used to calculate the average catalyst temperature plotted in Figure 3. Previous tests of PARs in Surtsey showed that the average catalyst temperature increased about 96° for each 1 mole % increase in vessel hydrogen concentration when the PAR is operating at steady-state (Blanchat 1998). Note that the catalyst temperature spiked at about 4.3 hours, due to the suspected hydrophobic coating burn off. Note also that catalyst heating was not uniform. The top of the cartridges showed delayed heating early in the test and there were large temperature differences at peak operation. Close inspection of Figures 3 and 4 reveal that the center cartridges were hotter than the cartridge near the PAR wall. The temperature of the cartridge usually increased from the bottom to the top. Uneven heating has been seen on other tests.

Figure 5 shows the PAR inlet and outlet (measured at the chimney exit) temperatures from the thermocouples located in the middle and near the edge of the PAR along with the gas addition flow rates as measured from the hydrogen and oxygen flow controllers. The temperatures at the chimney exit were mostly uniform except during startup, where the edge temperatures were slightly higher than the centerline temperatures. Oxygen was added at half the hydrogen rate to maintain a relatively constant oxygen level.

Figure 6 compares vessel pressure and saturation pressure (using the array B average temperature and saturated steam tables) to the steam and the relative humidity fraction. The relatively humidity increased from 40 % to 100 % and the maximum steam concentration reached about 2 % at about t = 5 hours (due to the operation of the PAR). The slight pressure increase during the course of the test was due to the vessel average temperature increase (again, caused by the PAR operation). The infrared camera was not

operational during PP-1. The view from the CCD camera was uneventful. The view was mostly clear during the first five hours, becoming foggy after that time. No white particles were seen floating in the Surtsey vessel.

Figure 7 shows the velocity of the gas (in meters per second) at the PAR chimney exit using the hot-wire anemometer and the pitot-tube differential pressure transducers. The velocity measurements are discussed in greater detail in a following section. Figure 7 also shows the location of the velocity instrumentation (based on the x-y translator motor position) during the chimney traverses. When not being traversed, the instrumentation was located at the center of the chimney exit (position 40, see Figure 13). In addition, Figure 7 also shows a prediction of velocity based on the difference between the PAR inlet and outlet temperature (discussed below), and mixing fan operation.

The next five figures focus on gas concentration measurements. Figure 8 shows the dry-basis gas concentration at the PAR inlet sample point as determined from the real-time gas mass spectrometer. Figure 8 also presents the gas grab sample (GGS) post-test measurements. The GGS measurements compared very well to the mass spectrometer results. Also, hydrogen concentration estimated using temperature correlations (34 K PAR ΔT / 1% H_2, 96 K catalyst temperature increase / 1% H_2) gives confidence that the mass spectrometer results are correct (see Figure 8). The PAR ΔT (differential temperature) was calculated from the difference of the PAR outlet and inlet average temperatures (see Figure 5).

Figure 9 gives the wet-basis concentrations of hydrogen, oxygen, nitrogen, and steam (also at the PAR inlet sample point). Note that with the steam concentration reaching only about 2 mole %, the wet-basis concentrations are very close to the dry-basis values. Figure 10 focuses on the wet-basis hydrogen concentrations at the vessel floor, PAR inlet, PAR outlet, and vessel dome locations. This figure also shows the integrated hydrogen addition in total moles as a function of time. The hydrogen concentrations at the floor, PAR inlet, and dome are essentially identical throughout the test. This indicates that the mixing fans maintained the vessel in a well-mixed condition.

Figures 11 and 12 compare hydrogen and oxygen wet-basis concentrations (at the PAR inlet) and integrated hydrogen and oxygen additions to either the average catalyst temperature or the PAR ΔT.

One unexpected result occurred. The PAR startup was not as quick or robust as in previous tests with fresh cartridges in non-steam atmospheres. After the first hydrogen addition, the hydrogen concentration was 0.5 mole % at about t = 0.4 hours. Immediately before the second hydrogen addition (at t = 1.4 hours), the PAR catalyst temperature increase was only about 6 K and the PAR ΔT was about 3 K. This was well below the PAR catalyst temperature increase of 35 K and the PAR ΔT of 15 K, seen in both the PAR-1 and the PAR-2 experiments. The hydrogen concentration at the PAR outlet showed almost no decrease (compared to the inlet concentration), another indication of

the weak startup. The PAR started quickly after the second add at 1.4 hours to a hydrogen concentration of 1 mole %.

Velocity Measurement and Prediction

Figure 13 converts the motor position to a location in x (positions 32-48) and y (positions 49-63) as the instrumentation traversed the chimney exit. The tip of the hot-wire stops at each motor position. The stepper motors moved the two pitot tubes and the hot-wire anemometer (drawn approximately to scale) in ½ inch increments, with the hot-wire about 1 inch to the chimney walls. Note that the pitot-tubes measure flow about 0.7 inches on each side of the hot-wire. The instrumentation was normally parked at the chimney center (location 40). During a traverse, the instrumentation would move left to position 32, then traverse right in the x-direction from position 32 to position 48, then left back to position 40 and then down to position 49 to start the traverse in the y-direction. After traversing in y from position 49 to position 63, the instrumentation would move in y back to position 40. Typically, a twenty second measurement was made at each position.

Figures 14 through 16 show the flow velocity and the motor position during the four traverses: starting at about 5.4 hr., 5.9 hr., 6.4 hr., and 7.4 hr. The mixing fans were operated prior to each traverse to ensure well-mixed conditions. The velocity measured by the anemometer seemed low when compared to that measured by the pitot tubes. This is especially evident in Figure 7, except at the peak PAR operation. Discussion with the manufacturer to determine the cause revealed that the anemometer was incapable of accurately measuring velocities less than 0.5 m/s. While explaining the anemometer behavior shown in Figure 7, it became obvious that the anemometer data was in error over most of the PAR flow range. Therefore, the pitot tube data was solely used in the determination of the PAR flow.

As mentioned earlier, the PAR flow can be calculated as a function of the temperature rise through the PAR. Integration of the Bernoulli equations in a loop up through the PAR and then down outside the PAR back to the inlet yields the equations of flow, yielding essentially a balance between buoyancy forces and flow losses in the PAR.

The ambient fluid outside the PAR has constant temperature, approximately equal to the PAR inlet temperature. The temperature inside the PAR increases approximately linearly as it rises through the catalyst plates, is relatively constant as it rises in the chimney, and then the gas discharges as a buoyant jet with a temperature greater than the ambient temperature outside the PAR. The net buoyant force is

$$\Delta P = \Delta\rho \; g \; (H_c + \frac{1}{2} H_p) = \Delta\rho \; g \; H_{eff} \qquad (1)$$

where

ΔP = differential pressure between chimney inlet and outlet

$\Delta\rho$ = density difference between the fluid outside the chimney and the buoyant jet

g = gravitational constant (9.81 m/s^2)
H_c = height of the chimney above the plates (0.8 m)
H_p = height of the plates (0.2 m)
H_{eff} = effective height of the PAR (0.9 m).

Since the effect of the composition change from the hydrogen combustion on the density is small, the density difference occurs due to the temperature change, therefore,

$$\Delta\rho = \rho \frac{\Delta T}{T} \tag{2}$$

where
ρ = average mixture density
ΔT = temperature difference between PAR inlet and outlet
T = PAR average absolute temperature.

The loss coefficients have been estimated using fluid dynamics textbooks and the Crane pipe design handbook. The flow losses occur due to contraction entrance losses entering the catalyst plate slots (k_{inlet} = 0.5), friction losses for flow along the slots (k_{slot} = 2.0), exit losses from the slots due to the sudden area expansion ($k_{slot\ exit}$ = 0.6), contraction losses due to the chimney transition ($k_{transition}$ = 0.3), and the losses due to the sudden area expansion at the chimney exit (k_{exit} = 1.0). The total loss coefficient, k, is estimated to be 4.4. Note that it is possible to directly determine the loss coefficients through isothermal forced convection measurements of ΔP versus volumetric flow rate.

The total volumetric flow, Q, is then given by

$$\Delta P = \frac{1}{2} k \rho V^2 = \frac{1}{2} k \rho \left(\frac{Q}{A}\right)^2 \tag{3}$$

where
A = PAR exit flow area (0.059 m^2).

Rearranging Equations 1,2, and 3 yields the velocity prediction.

$$V = \left(2 g \frac{h_{eff}}{k} \frac{\Delta T}{T}\right)^{\frac{1}{2}} \tag{4}$$

The velocity prediction based on Equation 4 is plotted on Figure 7, and also on Figures 14 through 17. The estimate of 4.4 for the total loss coefficient is probably close, since the velocity prediction is in good agreement with the velocities determined using the pitot tube instruments. The pitot tube data was qualified by a posttest calibration of the pitot tube gages.

Figure 18 plots flow velocity from each instrument during each traverse as a function of motor position. Since all velocity-time data was referenced to the motor position for the anemometer (HW11), the pitot tube locations have been adjusted to show their actual location in motor position units during the traverse in x (i.e., PT12 = HW11 - 1.4, PT13 = HW11 + 1.4). Above the plot are side and top views of the PAR, allowing a visual reference of the instrument locations in x and then y during the traverse. Figures 19 through 21 show the PAR flow velocity from the hot-wire, pitot-tube 12, and pitot-tube 13, respectively, at each traverse. These figures show the gas velocity decreasing as a function of time due to the PAR slowing down as the hydrogen concentration decreases.

Figures 22 through 24 compare the flow velocities measured by the three instruments at 5.4 hr., 5.9 hr., 6.4 hr., and 7.4 hr. Two observations can be made. The flow profile in x showed a double-hump profile, with lower flow at the center and the two walls. The flow profile in y showed a single peak off chimney centerline, skewed toward the PAR center. Remember that for the y-traverse, the motor position gives the *hot-wire* location; the pitot-tubes are located about 1.4 motor location units on each side of the hot-wire. Also, the hot-wire appeared to measure slightly lower velocities when compared to the pitot-tubes.

Flow Interpretation

Figures 19-21 show that about twenty measurements were performed at each location. A close inspection of the data showed that a steady-state had not been reached prior to the succeeding measurement, i.e., the time response of the pitot tubes was greater than the measurement interval. However, comparison with rate changes of the hot-wire (with its faster response) indicate that the pitot tube data probably was within ten percent of steady state. Therefore, a best fit of the data using the last measurement at each location was performed. These fits are given on Figures 22-25. The average of the two pitot tube fits were used to estimate the full-field velocity at the chimney exit (except at t = 7.4 hours, only the pitot tube 12 data was used since pitot tube 13 dropped out before the traverse). The hot-wire data was not used.

In order to determine the full-field velocity, it was assumed that the one measured velocity profile obtained during the x-traverse (at the centerline y position) could be replicated to produce velocity profiles at each y location by application of a shape function determined from the y-traverse velocity profile data. This function was simply a multiplier based on the ratio of the velocity measured at each y motor location divided by the velocity at the center location (motor position 56). The full-field velocity data thus obtained is plotted in Figures 26-29. The mean velocity across the full-field was then determined from the average of all position values.

Energy Balance

Once steady-state has been achieved, the energy release from the hydrogen combustion should balance the sensible heating of the volumetric flow through the PAR. This provides an independent way to verify the PAR flow through an energy balance. An estimate of the PAR heating from the hydrogen depletion rates is simply the hydrogen depletion rate times the enthalpy of reaction of hydrogen

$$q_{DPR} = DPR\ \Delta H_{hydrogen}\ 3600 s/hr \tag{5}$$

where
q_{DPR} = heating rate from hydrogen combustion (watts)
DPR = hydrogen depletion rate ((kg/hr)
$\Delta H_{hydrogen}$ = lower enthalpy of the reaction of hydrogen (1.19e08 J/kg).

Figure 30 presents the hydrogen depletion rate as a function of hydrogen concentration measured during the steady-state operation from 5.4 hours to the end of the test. The following procedure was used to determine the depletion rate. First, the time-dependent amount of hydrogen in the Surtsey vessel (in moles) was determined by multiplying the average hydrogen concentration by the total number of moles in the Surtsey vessel. The average hydrogen concentration was assumed to be that measured by the gas mass spectrometer at the PAR inlet sample point. The depletion rate was then determined by calculating the difference in hydrogen moles at each successive time interval, using data from the steady-state depletion interval, after the hydrogen additions were stopped.

The PAR heat generation rate, based on flow resistance and temperature drop, is

$$q_{sensible} = \dot{m} c_p \Delta T = \rho A V c_p \Delta T \tag{6}$$

where
$\dot{m}$ = mass flow rate of gas through the PAR (m^3/s)
ρ= average density of the gas mixture through the PAR (~2.5 kg/m^3)
A = flow area (0.059 m^3)
V = PAR gas flow velocity (m/s)
c_p = average specific heat of the gas mixture (~1.02 KJ/kg/K)
ΔT = temperature difference of the gas between PAR inlet and exit.

Equation 6 was implemented using velocities calculated by Equation 4, and gas mixture average properties determined from time-dependent gas temperature and concentrations measurements at the PAR inlet and exit. PAR heating rates from both methods are compared in Figure 31. Good agreement was obtained, providing confidence in the velocity prediction based on the PAR ΔT.

Gas velocity through the PAR as a function of hydrogen concentration in the Surtsey vessel is plotted in Figure 32. Figure 32 compares velocity during the PAR PP-1 experiment as calculated using the measured PAR ΔT to the velocity as measured with the pitot-tubes during the four traverses. The pitot tube data point at about 0.8 mole % hydrogen should be considered somewhat suspect, since one tube has already dropped out due to the low flow. A velocity correlation is also plotted, based on Equation 4 and assuming a temperature correlation (34 K PAR ΔT / 1% H_2) determined from previous experiments. The velocity correlation should be scale independent, i.e., the velocity for a full-scale PAR should be identical (assuming minor heat loss effects) to the 1/8 scale PAR (assuming an identical configuration to that PAR design tested at SNL)..

PAR volumetric flow rate is also plotted in Figure 32, essentially the velocity data times the flow area (0.059 m^2). Note that the flow rate correlation is scale dependent; the full-scale PAR volumetric flow rate should be approximately 8 times that seen in the PP-1 experiment.

Conclusions

The Surtsey test facility at SNL was used to determine if a catalyst temperature spike observed in previous tests was repeatable and to determine the flow characteristics of a 1/8 scale PAR at various hydrogen/air concentrations. As hydrogen was slowly injected into the Surtsey vessel, a temperature spike was observed at a hydrogen concentration of 1.6 mole % and a catalyst temperature of 460 K. This proved that the temperature spike is a repeatable event.

Hydrogen concentration was then increased to 3.5 mole %. As the PAR recombined and reduced the hydrogen gas in the Surtsey vessel, velocity measurements were taken at four different hydrogen concentrations. The velocity data were used to calculate the volumetric flow rate through the PAR as a function of hydrogen concentration. The data were used to develop a relationship to predict the flow velocity through the PAR as a function of the difference in temperature between PAR outlet and inlet. The PAR heating rate was then calculated using the velocity prediction. The PAR heating rate was also calculated using the energy release from the measured hydrogen combustion. Good agreement was obtained between the two independent energy methods, providing confidence in the velocity prediction based on the PAR ΔT.

References

Blanchat, T.K., and A. Malliakos (USNRC), "Performance Testing Of Passive Autocatalytic Recombiners," NUREG/CR-6580, SAND97-2632, Sandia National Laboratories, Albuquerque, New Mexico, 1998.

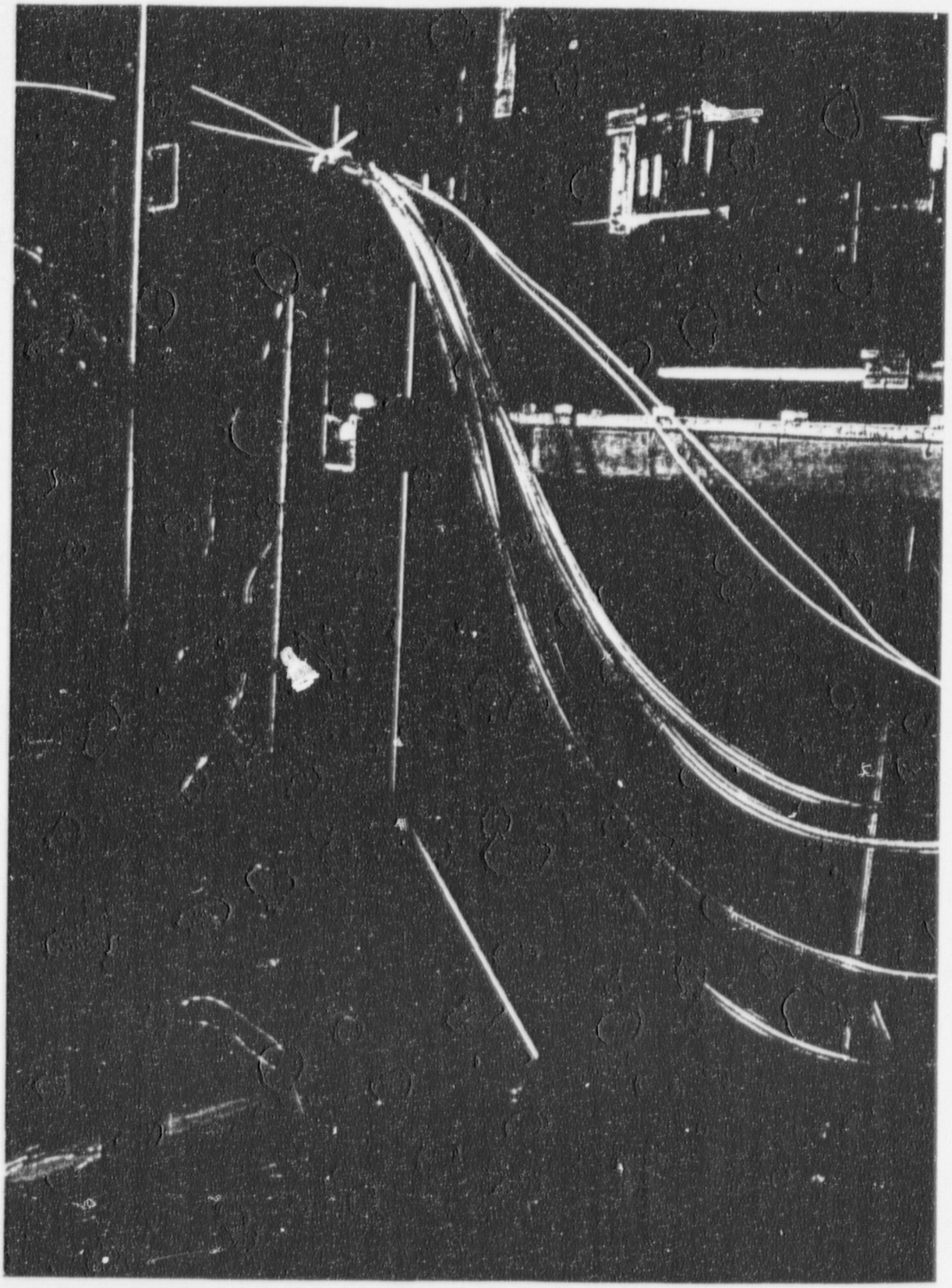

PAR side view.

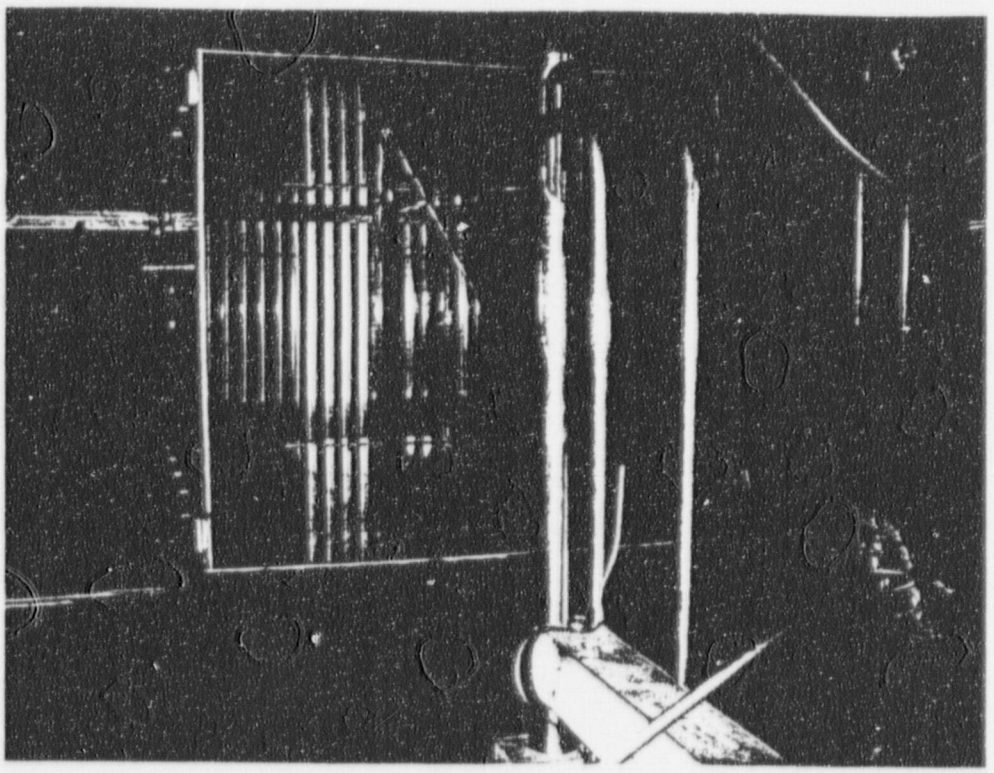

Top view of PAR at chimney exit.

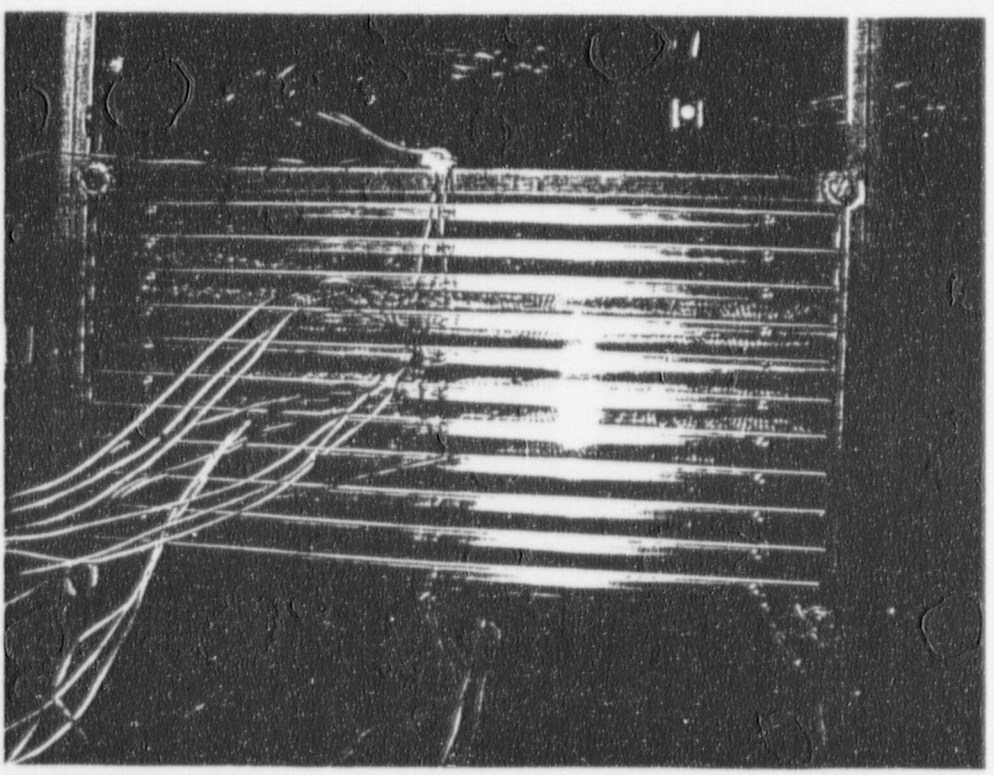

Bottom view of PAR inlet showing middle, edge, and corner thermocouples.

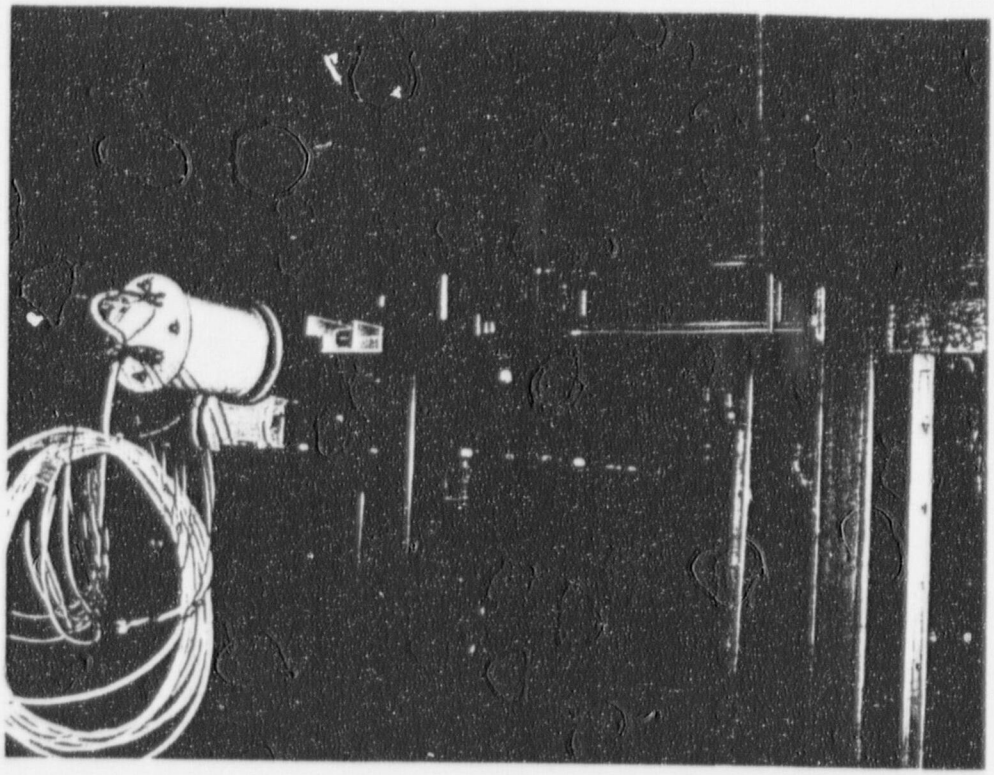

X-Y translator motors and tables mounted near chimney exit.

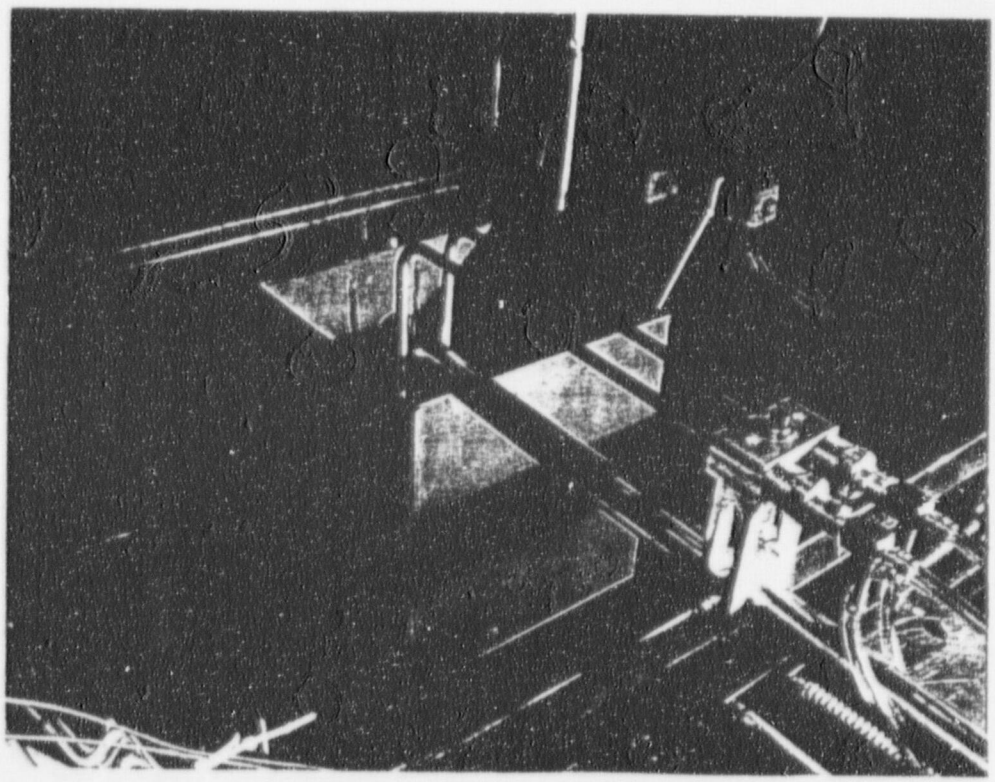

Pitot tubes and anemometer at the chimney exit

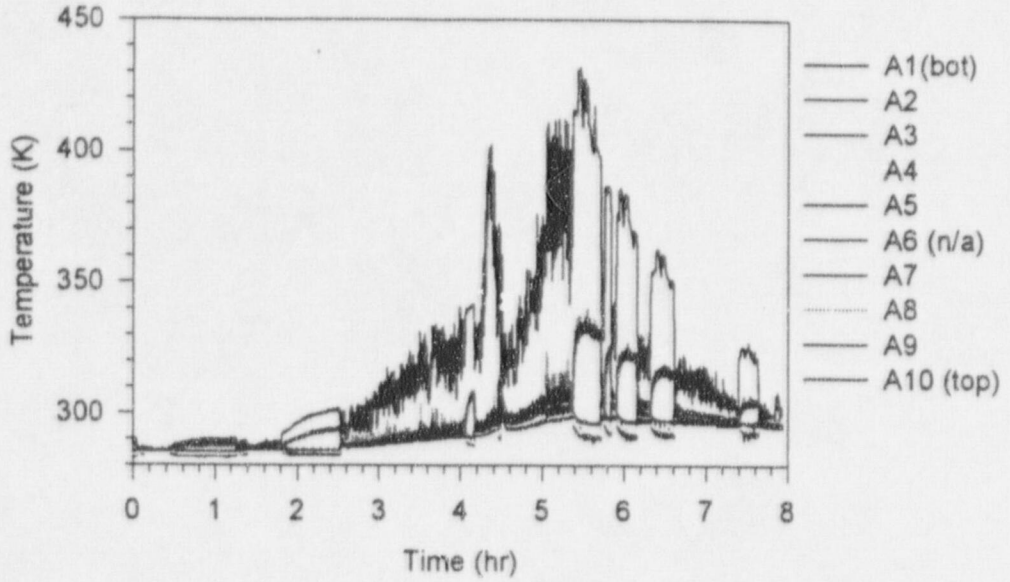

Figure 1. Surtsey vessel centerline gas temperatures from TC array A in PP-1.

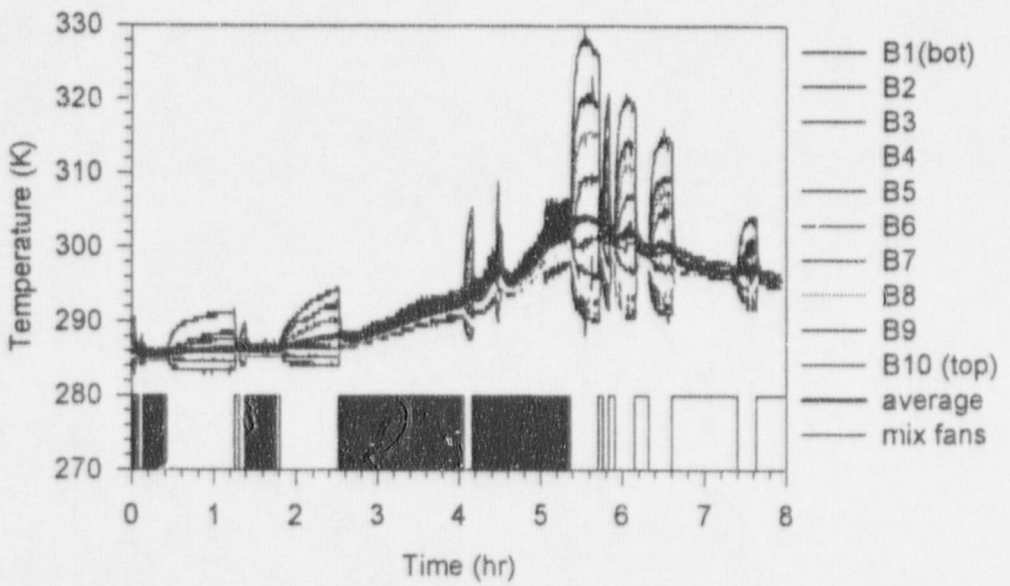

Figure 2. Surtsey vessel wall gas temperatures from TC array B in PP-1.

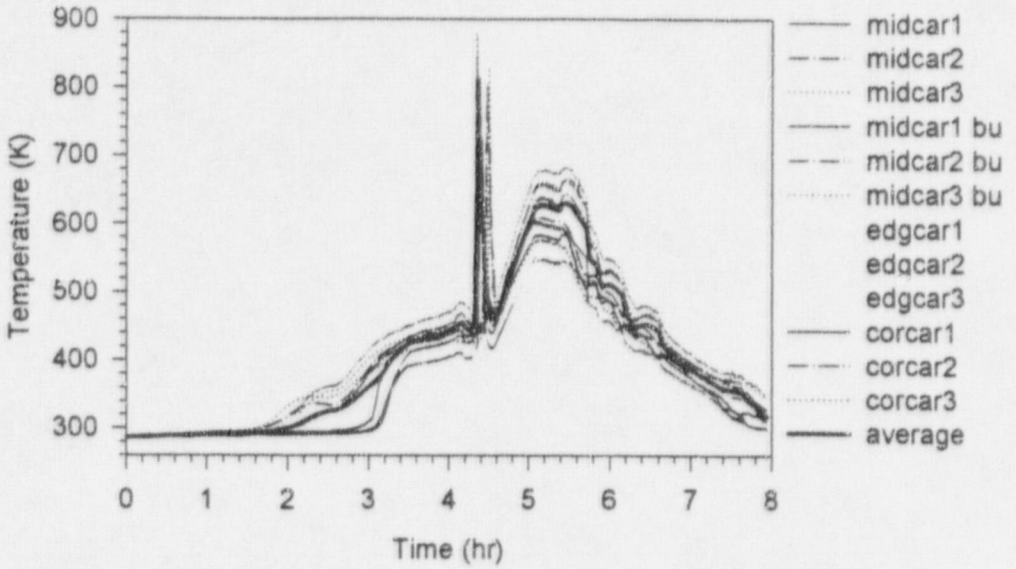

Figure 3. Catalyst cartridge temperatures in PP-1.

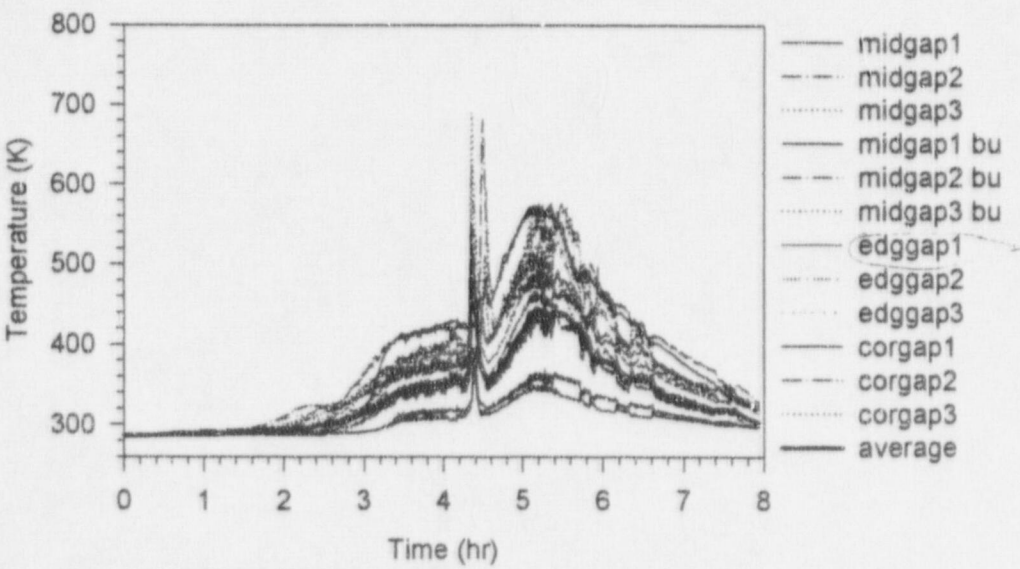

Figure 4. Catalyst gap temperatures in PP-1.

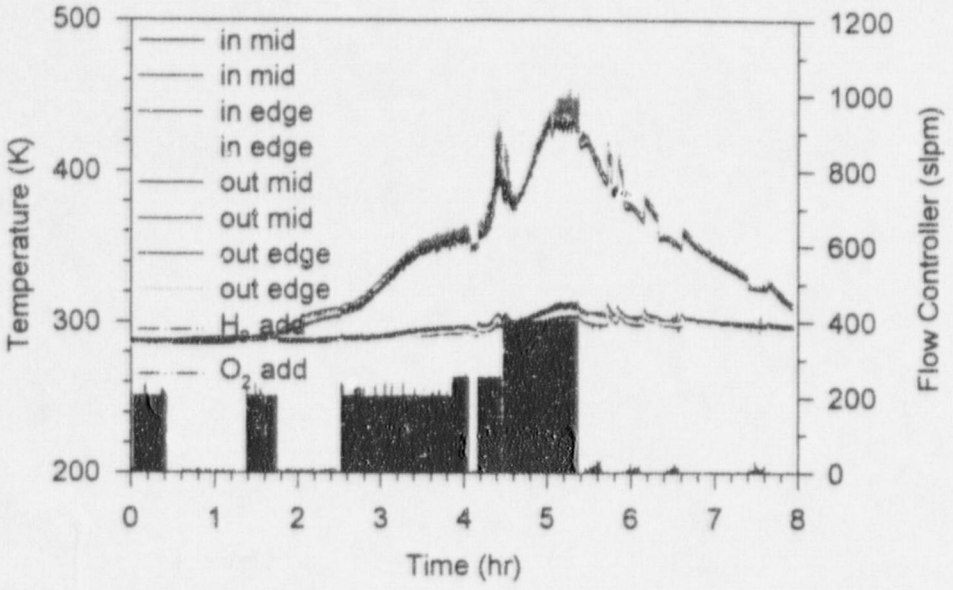

Figure 5. Inlet and outlet temperatures in PP-1.

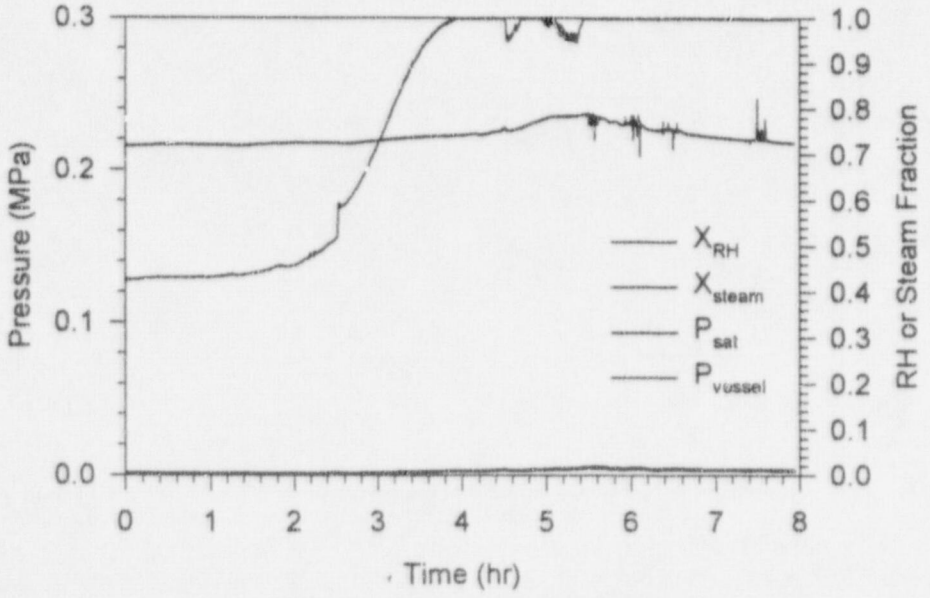

Figure 6. Saturation pressure, vessel pressure, relative humidity, and steam fraction in PP-1.

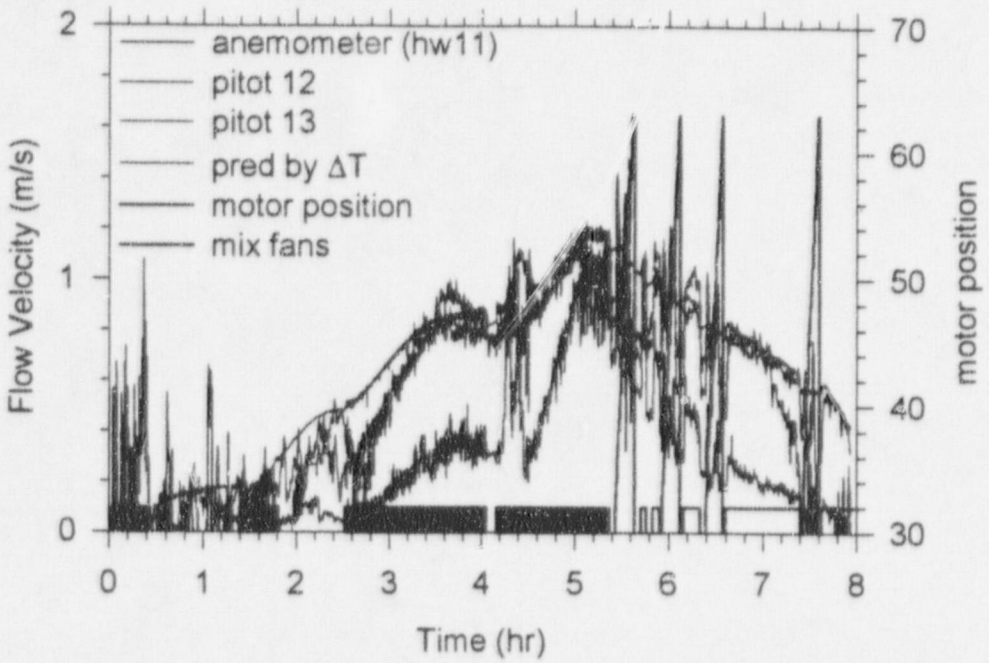

Figure 7. PAR gas velocity in PP-1.

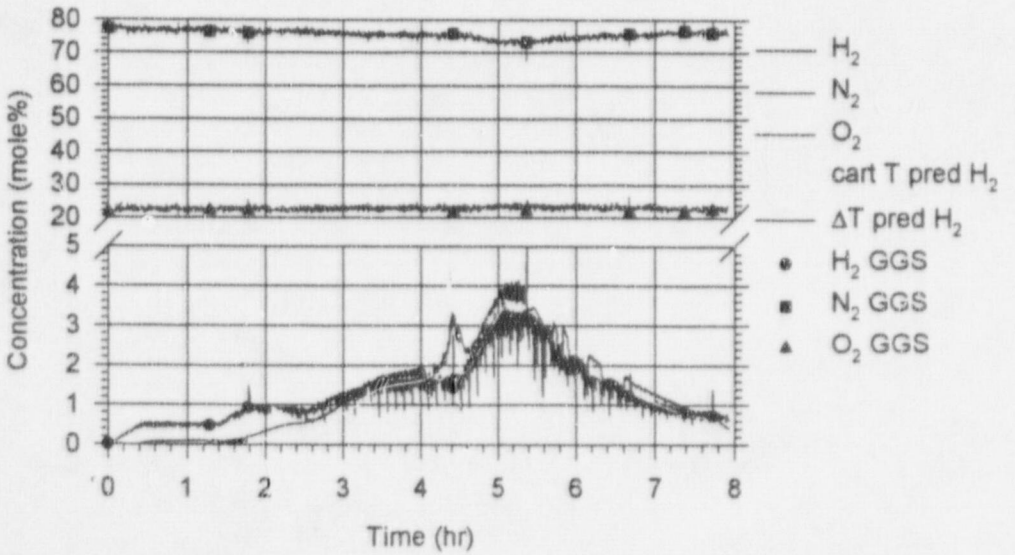

Figure 8. Gas concentrations (dry-basis) in PP-1.

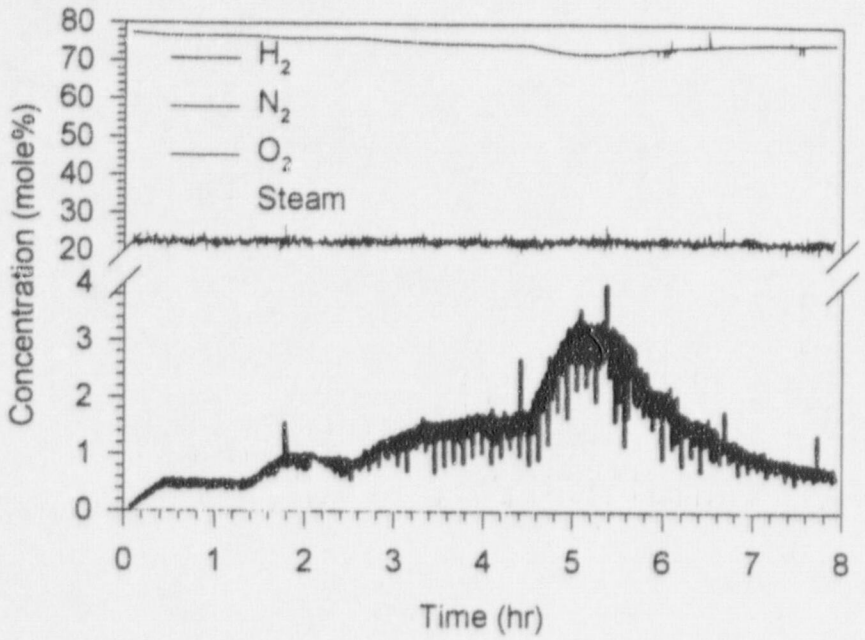

Figure 9. Gas concentrations (wet-basis) in PP-1.

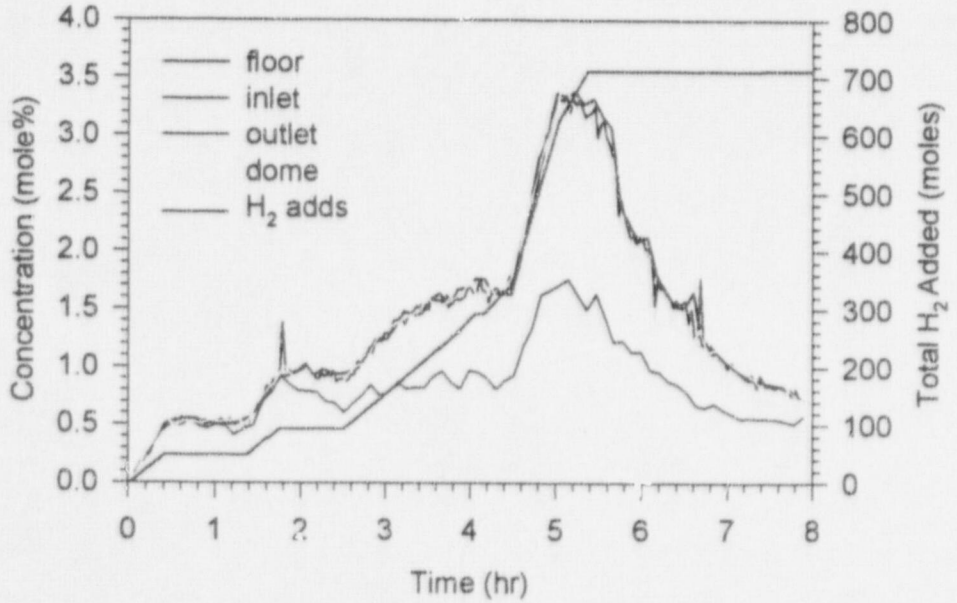

Figure 10. H_2 concentrations (wet-basis) in PP-1.

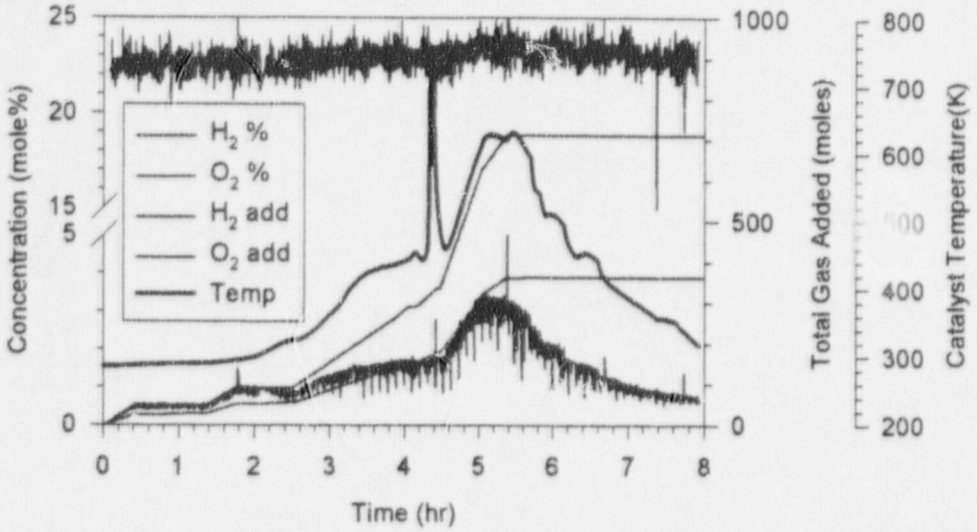

Figure 11. Catalyst temperature compared to gas additions and concentrations in PP-1.

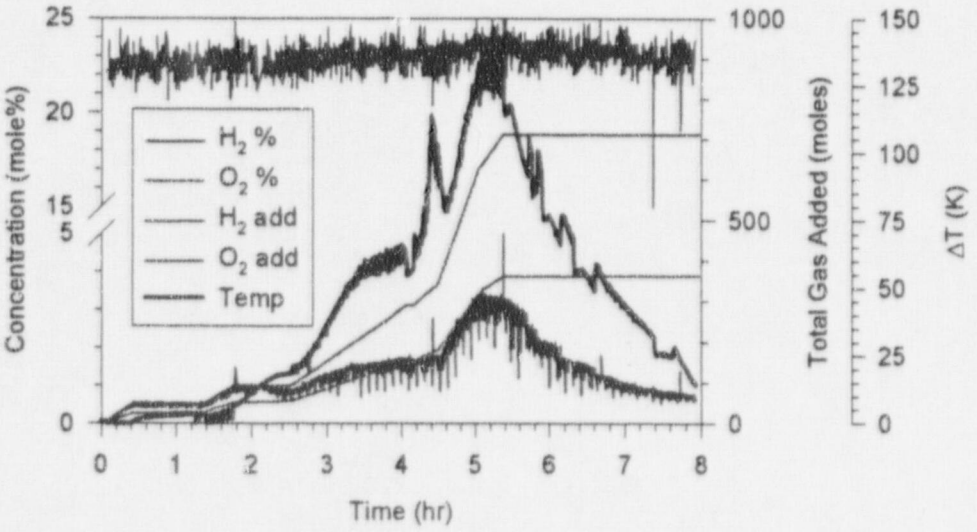

Figure 12. PAR ΔT compared to gas additions and concentrations in PP-1.

Figure 13. Motor position in x and y.

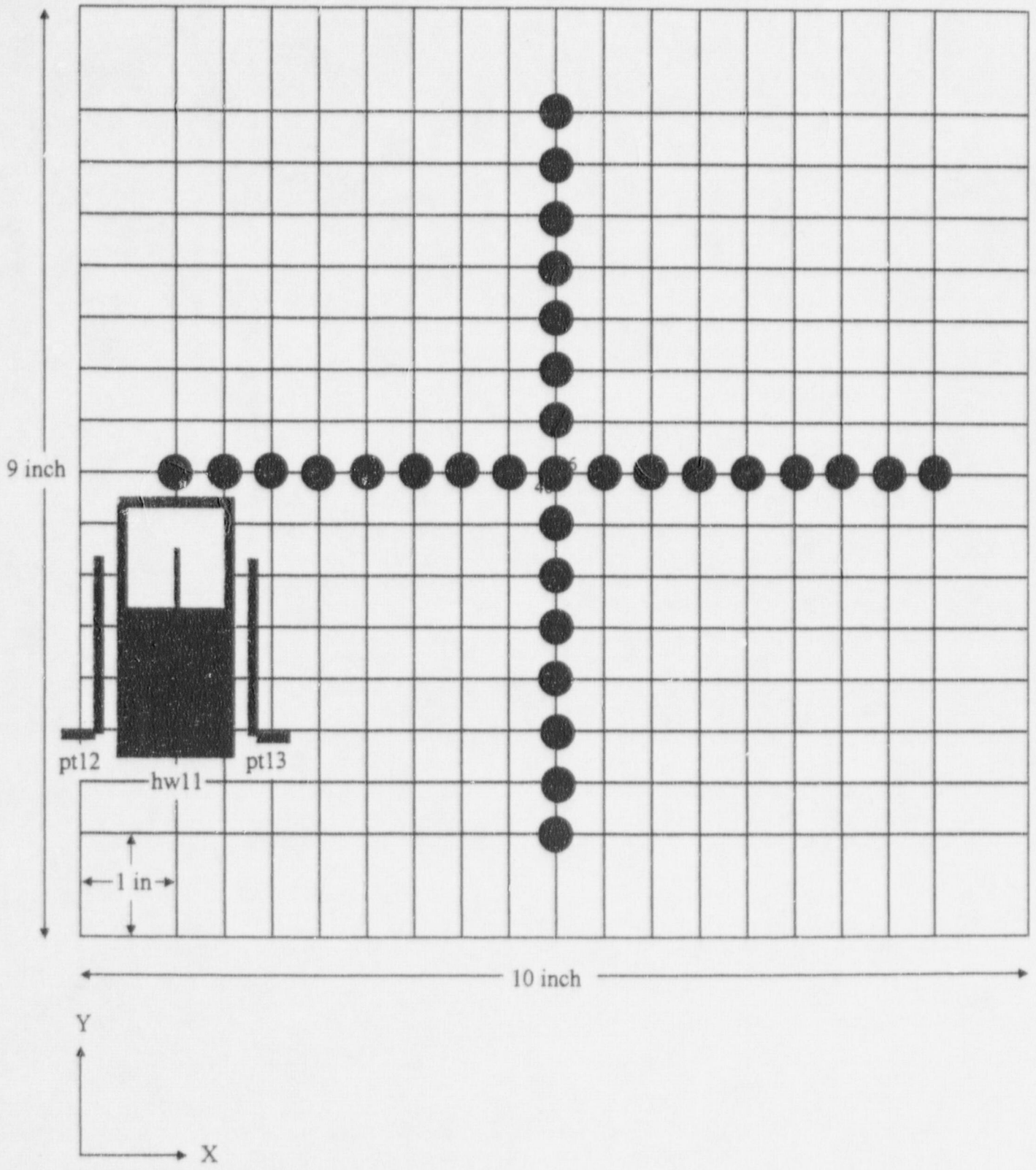

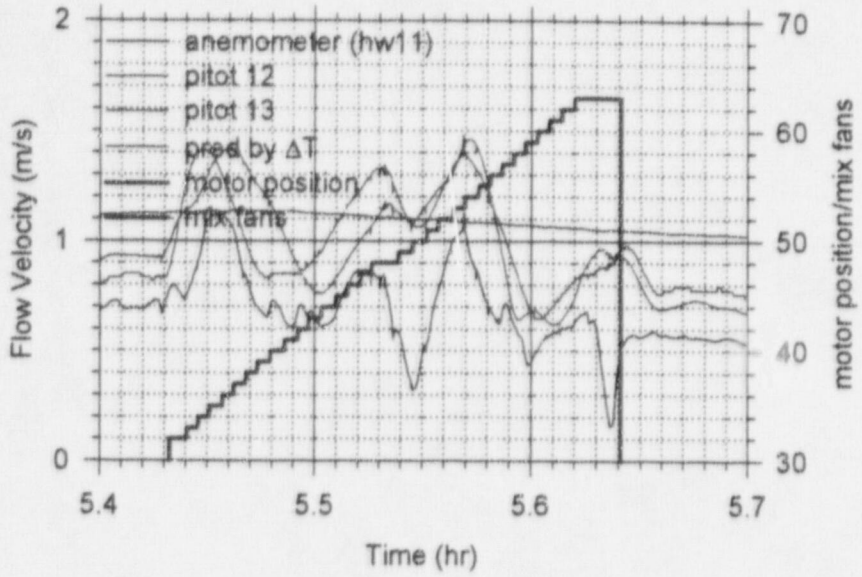

Figure 14. PAR gas velocity vs time in PP-1. (t = 5.4 hr)

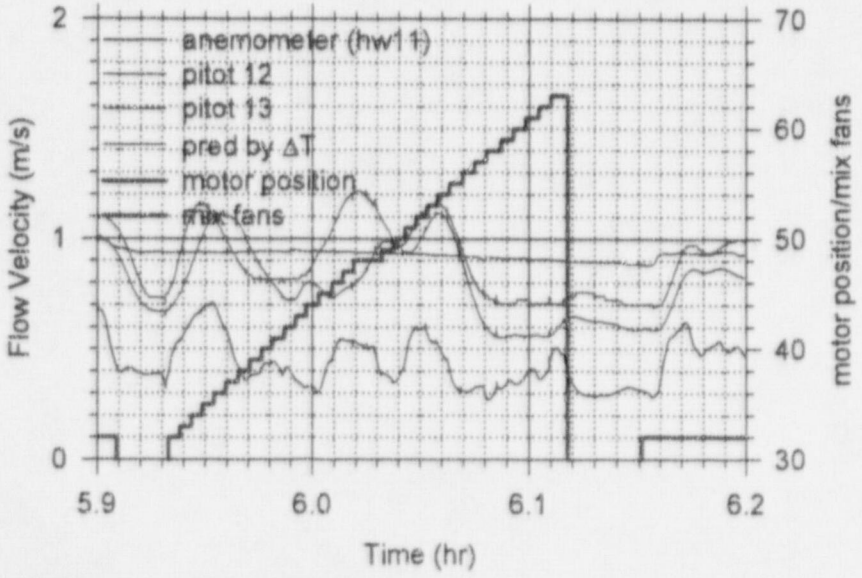

Figure 15. PAR gas velocity vs time in PP-1. (t = 5.9 hr)

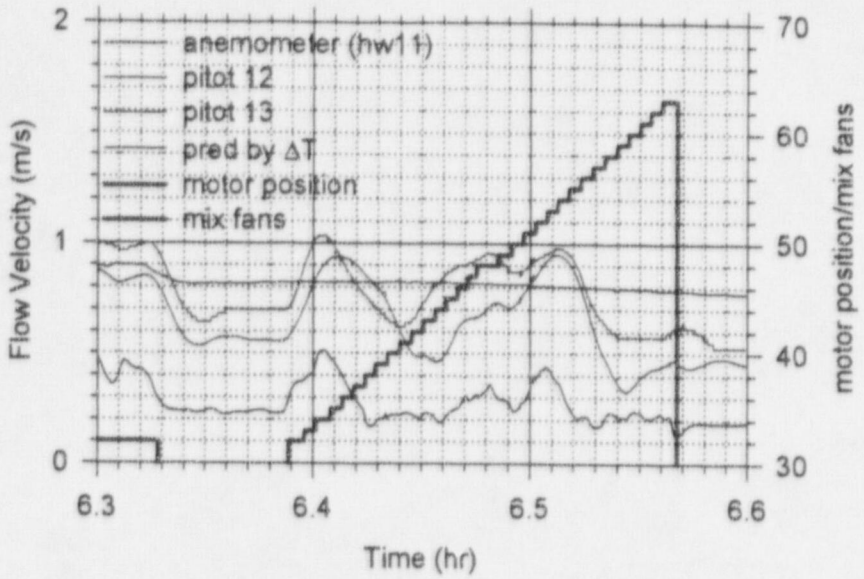

Figure 16. PAR gas velocity vs time in PP-1. (t = 6.4 hr)

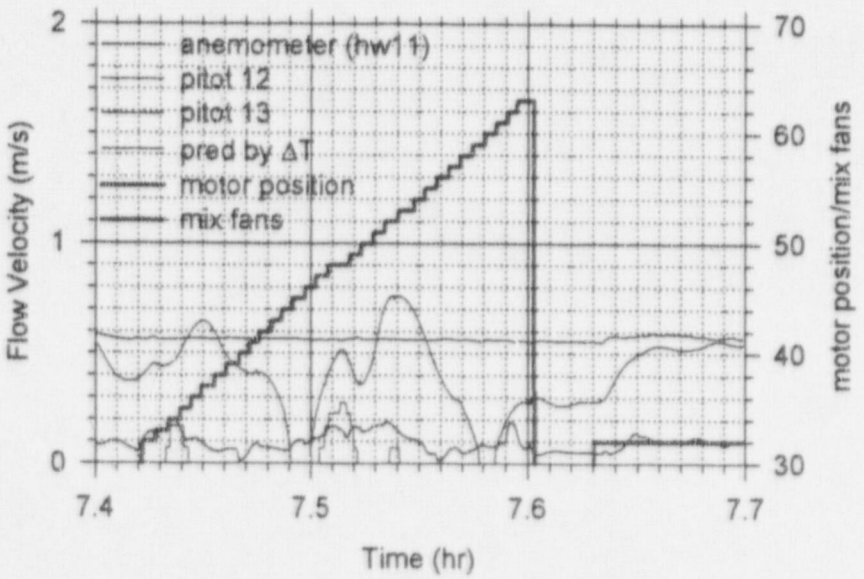

Figure 17. PAR gas velocity vs time in PP-1. (t = 7.4 hr)

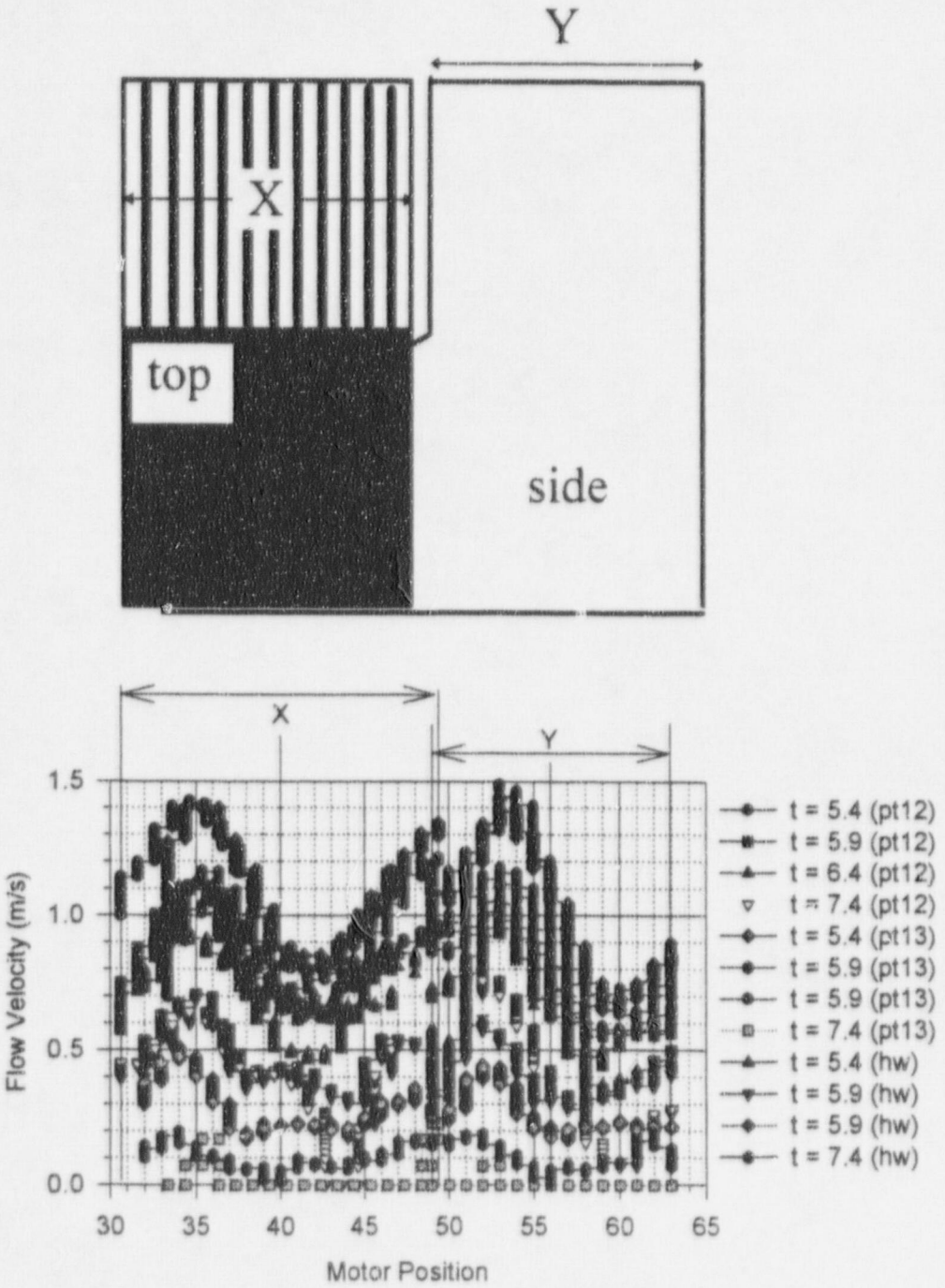

Figure 18. PAR gas velocity in PP1 (all).

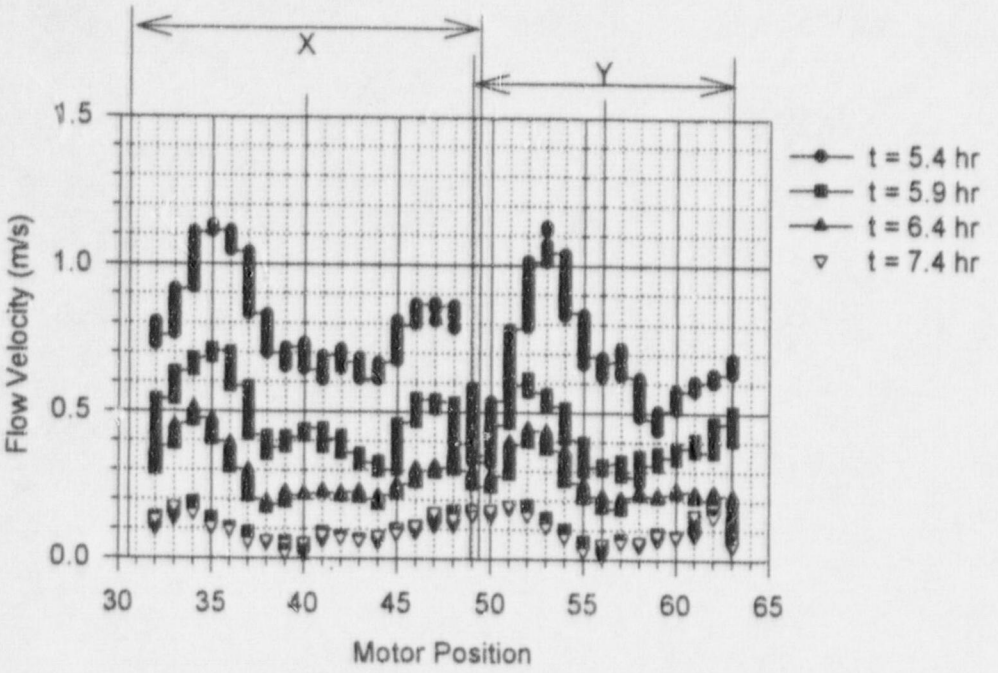

Figure 19. PAR gas velocity in PP-1 (HW11).

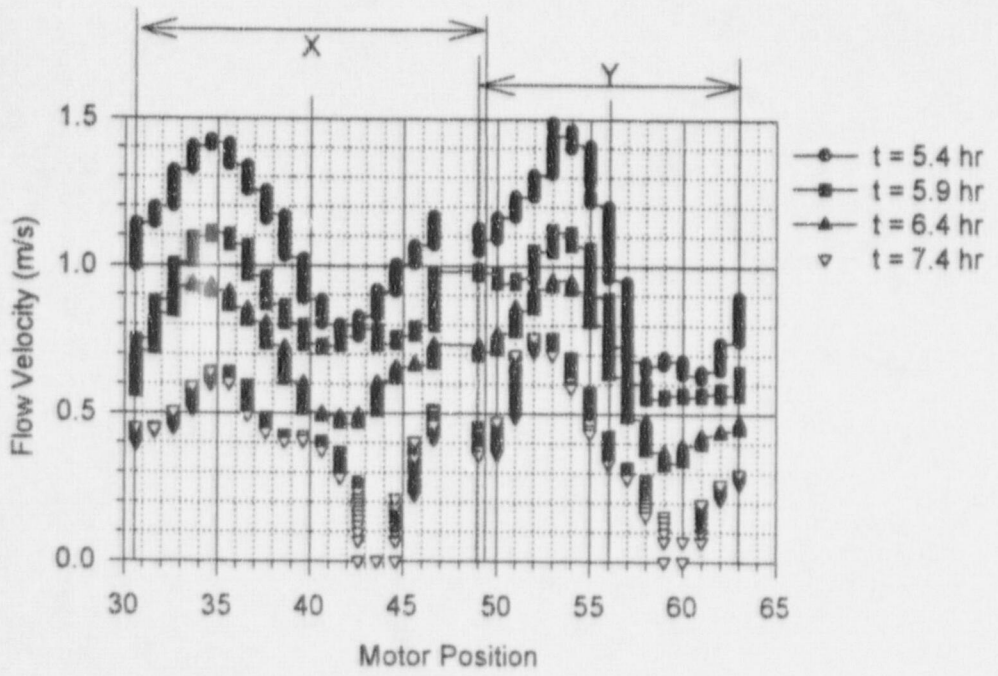

Figure 20. PAR gas velocity in PP-1 (PT12).

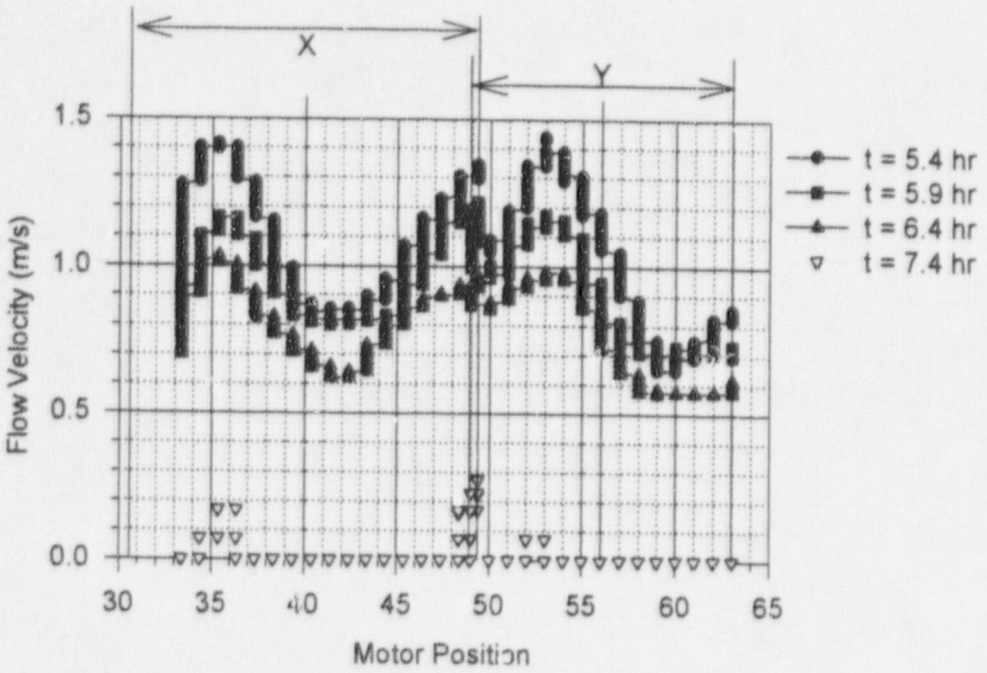

Figure 21. PAR gas velocity in PP-1 (PT13).

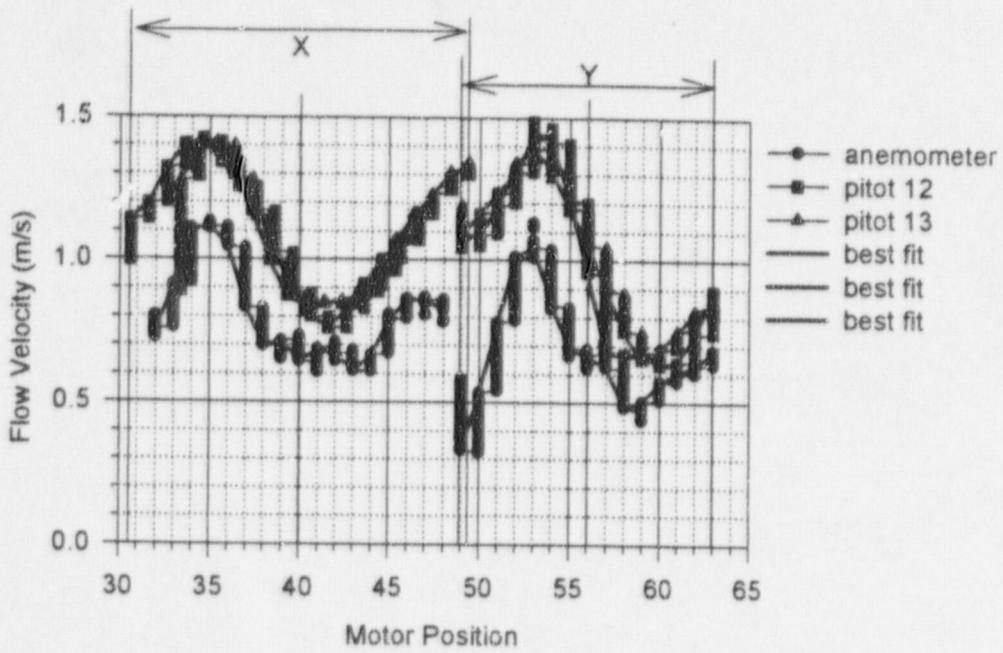

Figure 22. PAR gas velocity vs motor position in PP-1 (t = 5.4).

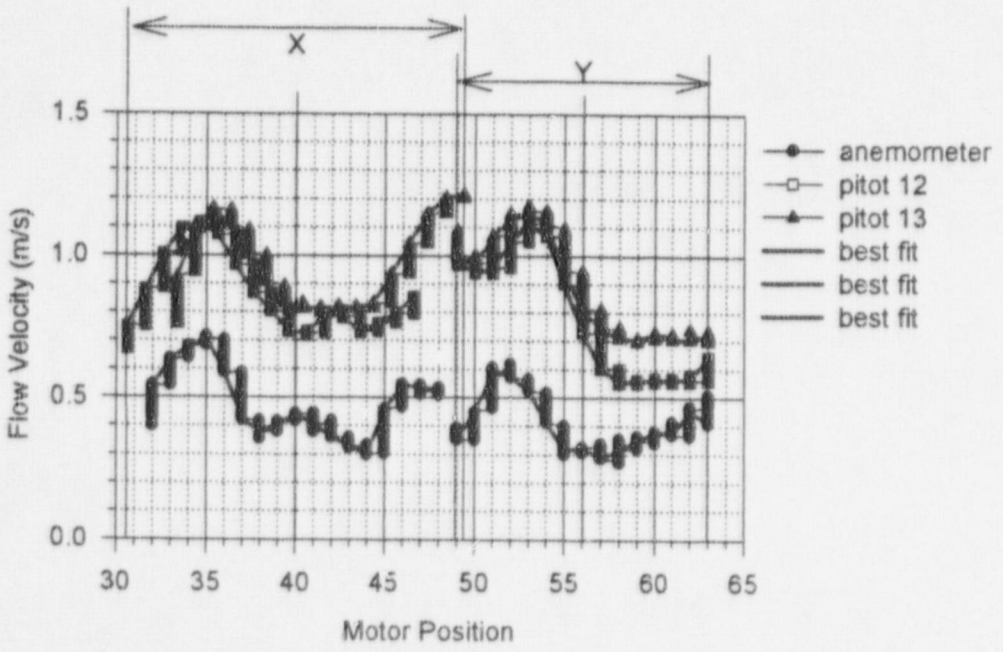

Figure 23. PAR gas velocity vs motor position in PP-1 (t = 5.9).

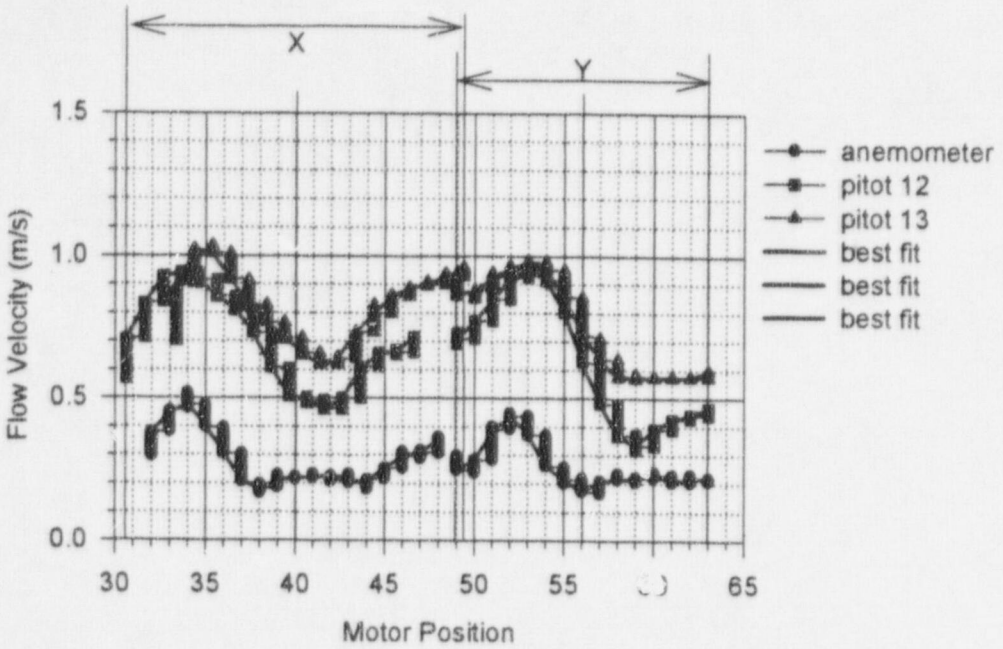

Figure 24. PAR gas velocity vs motor position in PP-1 (t = 6.4).

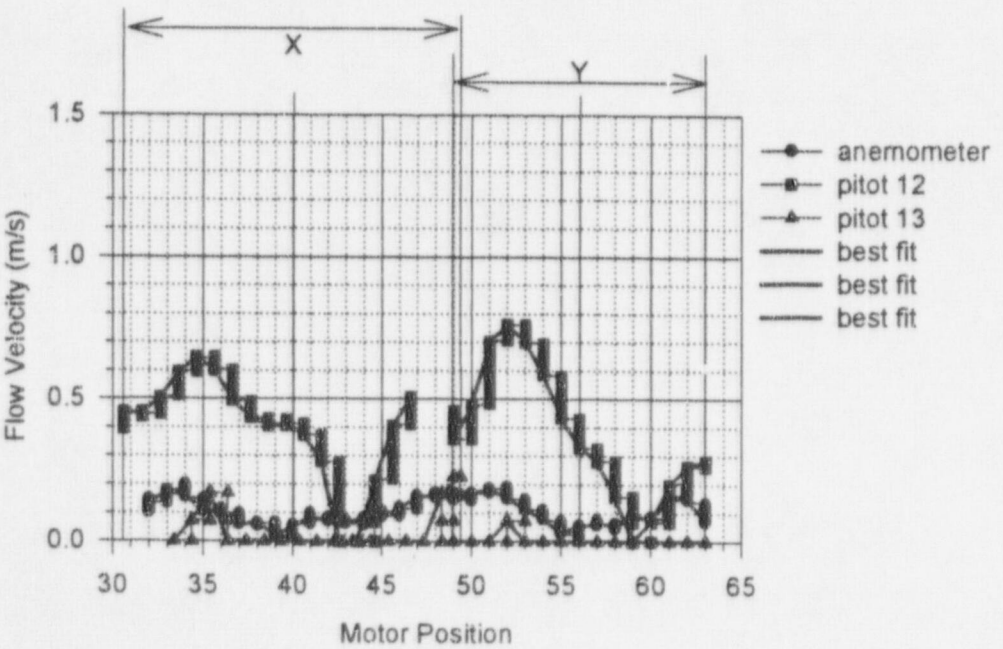

Figure 25. PAR gas velocity vs motor position in PP-1 (t = 7.4).

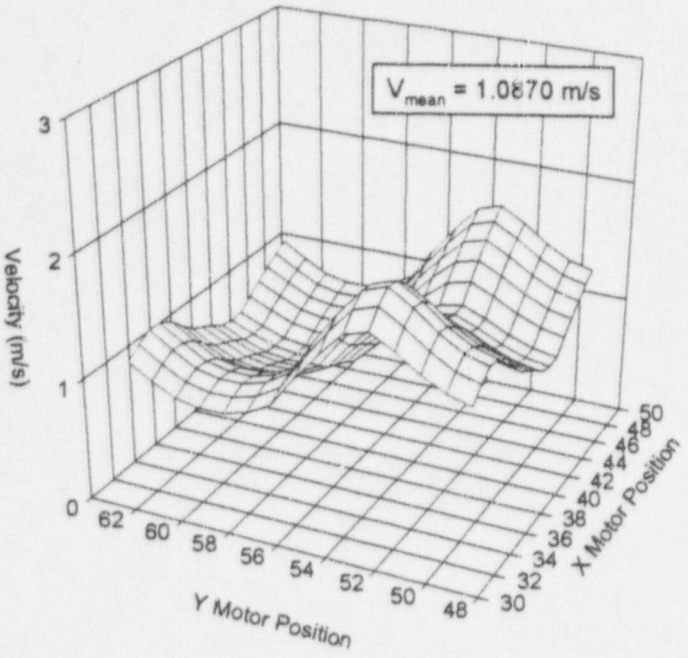

Figure 26. PAR chimney exit velocity at t = 5.4 hr.

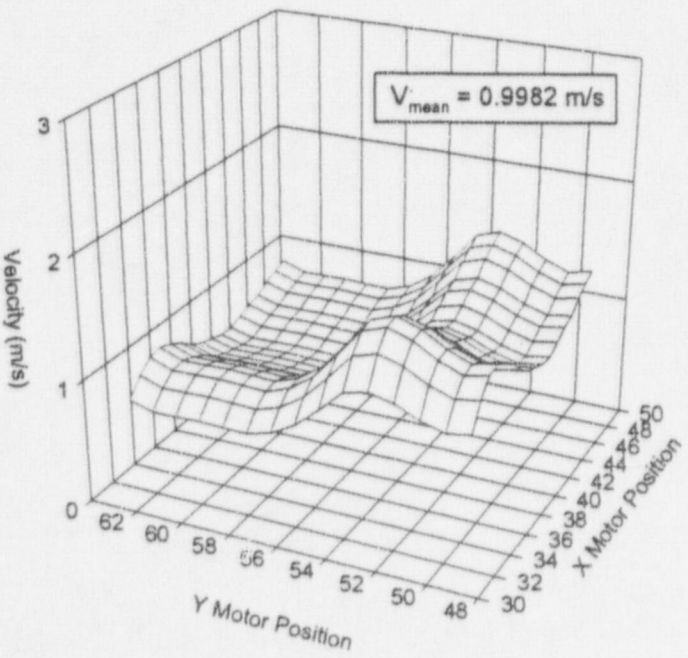

Figure 27. PAR chimney exit velocity at t = 5.9 hr.

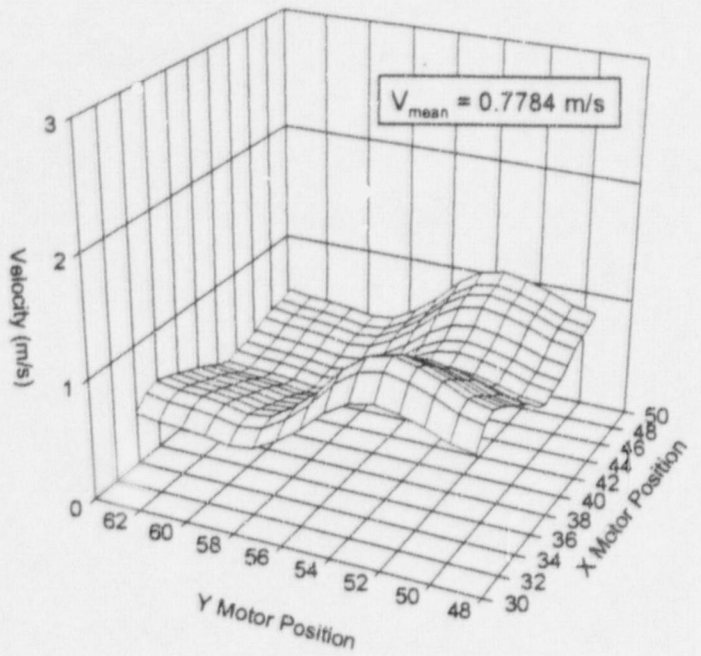

Figure 28. PAR chimney exit velocity at t = 6.4 hr.

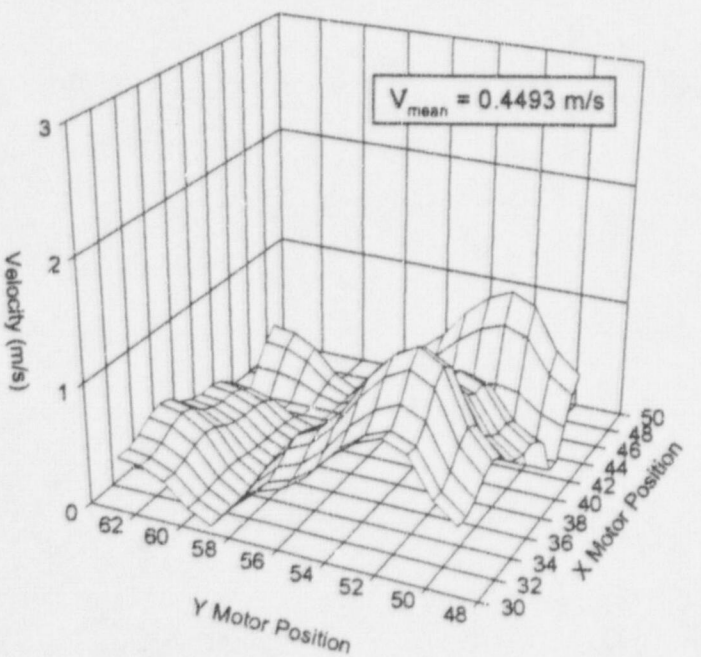

Figure 29. PAR chimney exit velocity at t = 7.4 hr.

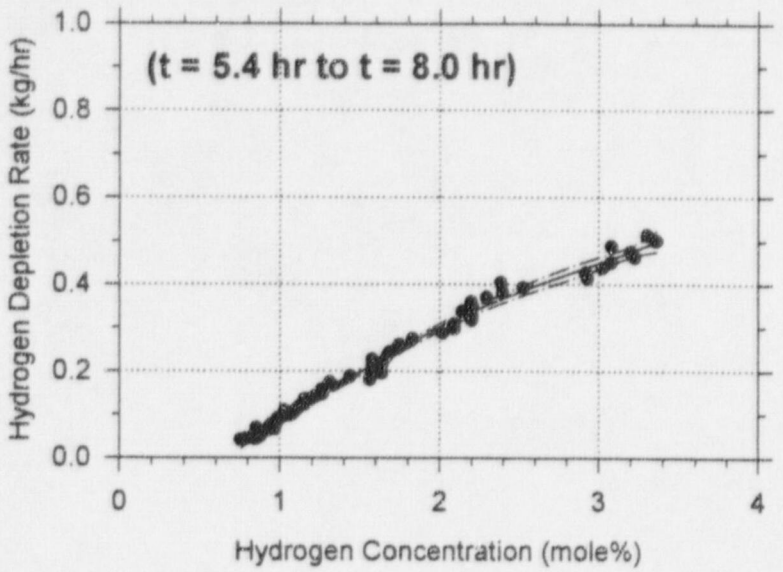

Figure 30. Depletion rate as a function of concentration.

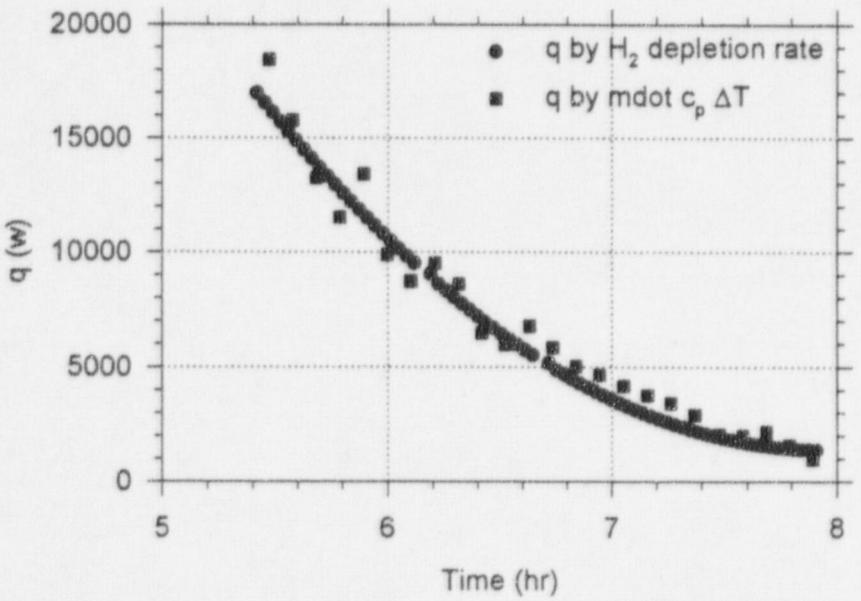

Figure 31. Heat addition comparisons: hydrogen depletion vs flow rate.

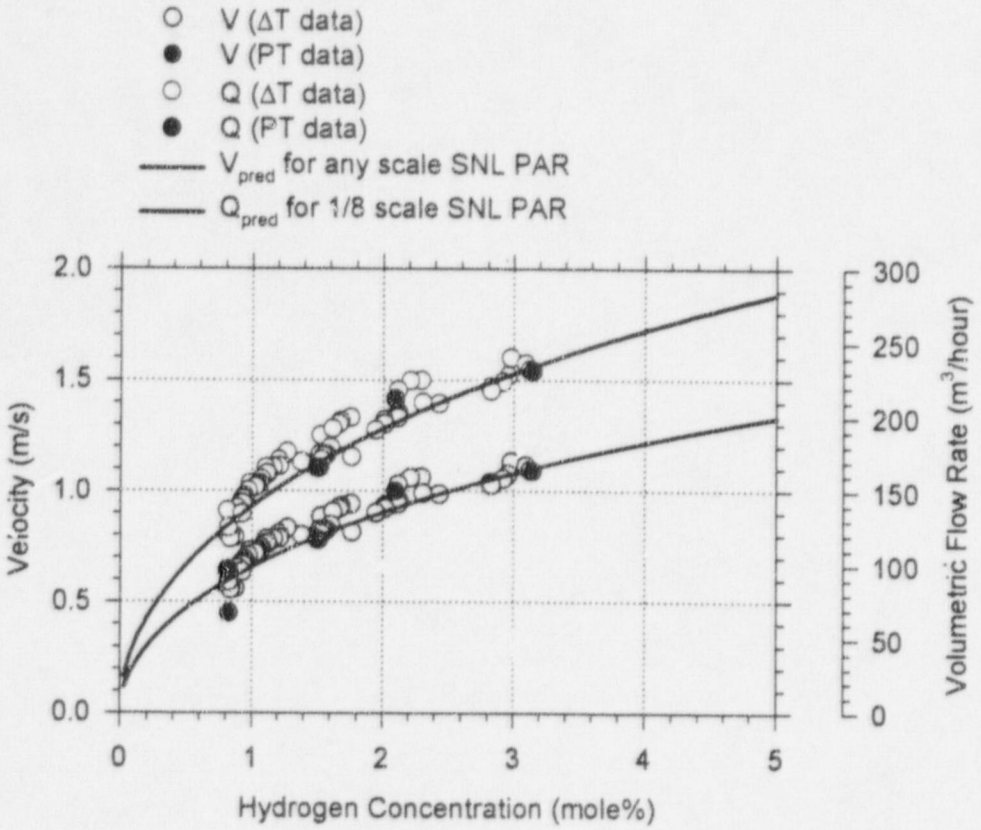

Figure 32. Flow and velocity measurements in the PP-1 experiment compared with 1/8 scale correlations.

Report on Ignition Behavior of PARs: The PP-2 Test

Background

The PP-2 PAR experiment performed in the Surtsey Test Facility was designed with two goals: 1) evaluate the characteristics of the PAR's ignition of hydrogen mixtures in an air/steam environment with *new* hydrophobic coating on the catalyst pellets and 2) evaluate the characteristics of the PAR's ignition of hydrogen mixtures in an air/steam environment with *destroyed* hydrophobic coating on the catalyst pellets. Both goals required well-mixed conditions. It was possible to meet both goals in one test since a catalyst temperature greater than 473 K was reached during the first ignition event (destroying the coating); subsequent ignitions were caused by catalyst with destroyed coating.

Note that the goal to perform a counterpart experiment to PAR-9 or PAR-14 (Blanchat 1998) and look for a catalyst temperature spike at about 473 K (suspected to be caused by the destruction of the hydrophobic coating) was achieved in both the PP-1 and PP-2 experiments.

Test Summary

The PAR was configured at 1/8 scale using new cartridges containing intact hydrophobic coating. The PAR was located at the centerline of the Surtsey vessel and about one meter above the false floor support I-beams. Pressure, temperature, and gas sampling instrumentation were as in previous tests, with the exception that the x-y translator table, hot-wire anemometer, lights, and hygrometer were either electrically disconnected or physically removed from the Surtsey vessel to ensure all extraneous electrical sources were removed. A charge-coupled device (CCD) video camera and an infrared (IR) camera recorded the PAR and surrounding views during the course of the test.

The Surtsey vessel was sealed and contained air at about 0.084 MPa. Steam was added until the vessel pressure was about 0.22 MPa and the temperature was 375 K. This yielded a steam concentration of 50 mole % and an air concentration of 50 mole %. Operation of the mixing fans ensured a well-mixed condition.

Hydrogen and oxygen gases were supplied to the vessel from separate manifolds. Standard 44 L compressed gas cylinders were installed on the manifolds. The cold gas entering the vessel was mixed with a small amount of steam using a diffuser/mixer pipe located near the floor of the vessel; this was necessary to prevent condensation of the steam. During most of the test, for every mole of hydrogen that was added, one-half mole of oxygen was also added. Mass flow controllers were used to provide precise metering of the hydrogen and oxygen into the vessel.

At the beginning of the test, about 200 moles of hydrogen were injected to achieve a hydrogen concentration of 2 mole % in the Surtsey vessel. The intent was to let the PAR start and reach the point where the new catalyst typically shows a spike increase in catalyst temperature, thought to be associated with the destruction of catalyst coating. Following the temperature spike, hydrogen was slowly injected (continuously increasing the hydrogen concentration) until ignition occurred. Following a brief pause to collect data and/or refresh the hydrogen manifold, the ignition cycle was repeated until the hydrogen gas supply (twenty 44L gas cylinders) was exhausted. Gas grab samples were taken prior to and immediately after most ignition events to verify the on-line gas mass spectrometer data.

Four ignition events occurred during the PP-2 experiment in well-mixed conditions:

Burn	Time (hours)	Hydrogen Concentration (mole %)	Catalyst Temperature (K)	Par Gas ΔT (K)
1	2.11	6.1	942	290
2	3.00	6.3	948	308
3	4.65	6.8	968	323
4	5.30	5.9	893	273
Average±S.D.		6.3±0.4	938±32	299±22

Measured Data

Figures 1 and 2 show the temperatures recorded by the centerline (array A) and the near wall (array B) vertical vessel gas thermocouple arrays. The time of the mixing fan operation is given on the array B plot (Figure 2). From the start of the test until about 5.4 hours, hydrogen and oxygen were added into the Surtsey vessel simultaneously with operation of the mixing fans. Temperature stratification occurred rapidly when the fans were not operating, indicated by the separation of temperatures at the different heights on the thermocouple arrays (for example, after 6.3 hours). Figure 2 also plots the average of the array B temperatures; this average vessel temperature was used with an ideal gas law calculation to determine the moles of gas in the vessel. The four burn times are easily seen by the average vessel gas temperature spikes seen in Figure 2.

Figures 3 and 4 show the cartridge catalyst and gap temperatures, respectively. Four specific points were instrumented: center of two middle cartridges (MIDCAR and MIDCAR BU), center of the wall cartridge (EDGCAR), and the corner of the same wall cartridge (CORCAR). The cartridge temperature (and corresponding gap) was measured near the bottom (location 1), in the middle (location 2) and near the top (location 3) along a vertical axis. The six middle cartridge thermocouples were used to calculate the average catalyst temperature plotted in Figure 3. Previous tests determined that the average catalyst temperature increased about 96 K for each 1 mole % increase in vessel hydrogen

concentration when the PAR is operating at steady-state. The catalyst temperature spiked at about 0.6 hours, suspected to be associated with the hydrophobic coating destruction. Figure 10 will show that the hydrogen concentration was close to 2.0 mole % at this time. Note also that catalyst heating was not uniform. There were large temperature differences at peak operation. Close inspection of Figures 3 and 4 reveal that the center cartridges were hotter than the cartridge near the PAR wall. The temperature of the cartridge usually increased from the bottom to the top.

Figure 5 shows the PAR inlet and outlet (measured at the chimney exit) temperatures from the thermocouples located in the middle and near the edge of the PAR along with the gas addition flow rates as measured from the hydrogen and oxygen flow controllers. In order to obtain a near steady-state concentration at the burn point and not overwhelm the PAR; the gas addition rates were slowly increased (based on depletion rate calculations) until the first burn (from 0.6 hours to 2.1 hours). The gas addition rates were kept constant for the subsequent three burns since the PAR was already hot. Oxygen was added at half the hydrogen rate to maintain a relatively constant oxygen level, except for a brief time at t = 5.7 hours. The mixing fans were running during all gas additions.

Figure 5 shows that the PAR startup was very quick. After the first hydrogen addition, the hydrogen concentration was 2.0 mole % at about t = 0.3 hours. The PAR started within ten minutes after reaching 2.0 mole % hydrogen, evident by the increase in PAR catalyst and gap temperature, the increase in the PAR gas outlet temperature, and the decrease in hydrogen concentration measured at the chimney exit.

Figure 6 compares vessel pressure and the steam fraction (calculated using the nitrogen-ratio method). Relative humidity was not measured since the hygrometer was disconnected to remove all potential ignition sources. The four burns caused pressure spikes of about 1-2 bars. The vessel pressure increased during the course of the test due to the gas additions and because of the increase in vessel average gas temperature caused by the strong PAR operation. The vessel was partially vented twice (at about 3.9 hours and 5.4 hours) to maintain pressure below 0.3 MPa during the test.

Figure 7 shows the velocity of the gas (in meters per second) at the PAR chimney exit using a pitot-tube differential pressure gage.

The next five figures focus on gas concentration measurements. Figure 8 shows the dry-basis gas concentration at the PAR inlet sample point as determined from the real-time gas mass spectrometer. Figure 8 also presents the gas grab sample (GGS) post-test measurements. GGS #5 was taken at the dome sample point, GGS #7 at the floor sample point; all other GGS were taken at the PAR inlet. The GGS measurements compared very well to the mass spectrometer results, with the exception that the GGS oxygen concentrations appeared to be about 2 mole % less than that determined by the real-time mass spectrometer.

Figure 9 gives the wet-basis concentrations of hydrogen, oxygen, nitrogen, and steam (also at the PAR inlet sample point). Note that with the steam concentration rose steadily, and reached about 70 % at the end of the test. In the PP-1 experiment, hydrogen concentration was estimated using the catalyst temperature correlation of 34 K PAR ΔT / 1% H_2. This PAR ΔT temperature did not work well at the high concentrations seen in this test. The correlation was revised using the data from this test and other pertinent tests (see Figure 13). The revised correlation gives a temperature increase of about 46 K for each 1 mole % increase. The hydrogen concentration estimated from this new correlation is also plotted in Figure 9.

Figure 10 focuses on the wet-basis hydrogen concentrations at the vessel floor, PAR inlet, PAR outlet, and vessel dome locations. This figure also shows the integrated hydrogen addition in total moles as a function of time. Note that the hydrogen addition rate was intentionally slowly increased as the first burn point was approached. The hydrogen concentrations at the floor, PAR inlet, and dome were essentially identical throughout the test. This indicates that the mixing fans maintained a well-mixed condition in the Surtsey vessel throughout the test.

Figures 11 and 12 compare hydrogen and oxygen wet-basis concentrations (at the PAR inlet) and integrated hydrogen and oxygen additions to either the average catalyst temperature or the PAR ΔT. The PAR ΔT (differential temperature) was calculated from the difference of the PAR outlet and inlet average temperatures (see Figure 5).

Note that a hydrogen burn did not occur at t = 6.15 hours, with a peak catalyst temperature of about 960 K and 7.8 mole % hydrogen. The gas mixture probably became nonflammable due to the steam concentration at 63 mole %.

Video Interpretation

Photographs of the test (selected images from the near-infrared (IR) camera video) are included with this report and their description is provided below. The view from both the IR and the charge-coupled device (CCD) cameras was black at the start of the PP-2 PAR test since the internal lighting was disconnected (to remove all potential ignition sources). The IR camera showed that the first burst of hot particles ejected from the chimney exit at about t = 1.3 hours (with catalyst temperature near 700 K and hydrogen concentration >3.5 mole %). This was followed by many repetitious bursts at few minute intervals until the first burn occurred. These particles remained suspended in the vessel and moved with the gas flow streams. At the time of the first burn, the PAR housing was clearly visible in the IR camera view due to internal heating. The hydrogen deflagration event was easily discernible by the IR camera since the deflagration was much hotter than the temperature of the glowing particles or the PAR housing (the intensity of the heat from the burn forced the electronic aperture to automatically stop down (partially close)). The CCD never saw the PAR body or the hydrogen combustion events, however, the burst of particles from the chimney exit and suspension of glowing particles in the Surtsey vessel were visible.

After a burn, the particles and the PAR housing disappeared from view as they cooled down with the decreased hydrogen concentration. As the hydrogen concentration increased prior to the next burn, the particles (and the repetitious particle burst events from the chimney exit) returned and got brighter in the camera views.

Five sets of photographs taken with the IR camera are enclosed, detailing the four burn events and a particle burst event that occurred about five minutes prior to the second burn event. The sequence details every fifth frame (0.017 s interval). The first burn appeared to start next to the PAR inlet. Burn 2 started in the middle of a cloud of hot particles that had erupted about 1 s earlier from the chimney exit. Burn 3 started near the false floor support I-beams. Burn 4 started far below the false floor support I-beams; the first indication of the burn was the radiant heating of the PAR body prior to seeing the flames rise from below into the camera view.

Conclusions

The Surtsey test facility at SNL was configured to evaluate the hydrogen ignition characteristics of a 1/8 scale PAR in a well-mixed air/steam environment with both new and used hydrophobic coating on the catalyst pellets. Hydrogen was injected at a rate slightly above the PAR consumption rate to slowly raise the hydrogen concentration in the Surtsey vessel to flammable levels. Four hydrogen deflagration events (burns) occurred in the Surtsey vessel. The burns occurred at closely repeatable conditions of hydrogen concentration and PAR temperatures. The PAR catalyst was new prior to starting this test. Due to the high temperatures from the first burn the catalyst coating was considered destroyed for the three subsequent burns.

Video from an infrared camera showed repetitious bursts of hot, glowing particles. The particles ejected from the PAR exit at few minute intervals at hydrogen concentrations higher than 3.5 mole % until a burn occurred. These particles floated in the vessel and moved with the gas flow streams. After each burn, the particles disappeared from view as they cooled down with the decreased hydrogen concentration. As the hydrogen concentration increased prior to the next burn, the particles became hotter and brighter in the camera view. The higher hydrogen concentration promoted new repetitious particle burst events from the PAR chimney exit.

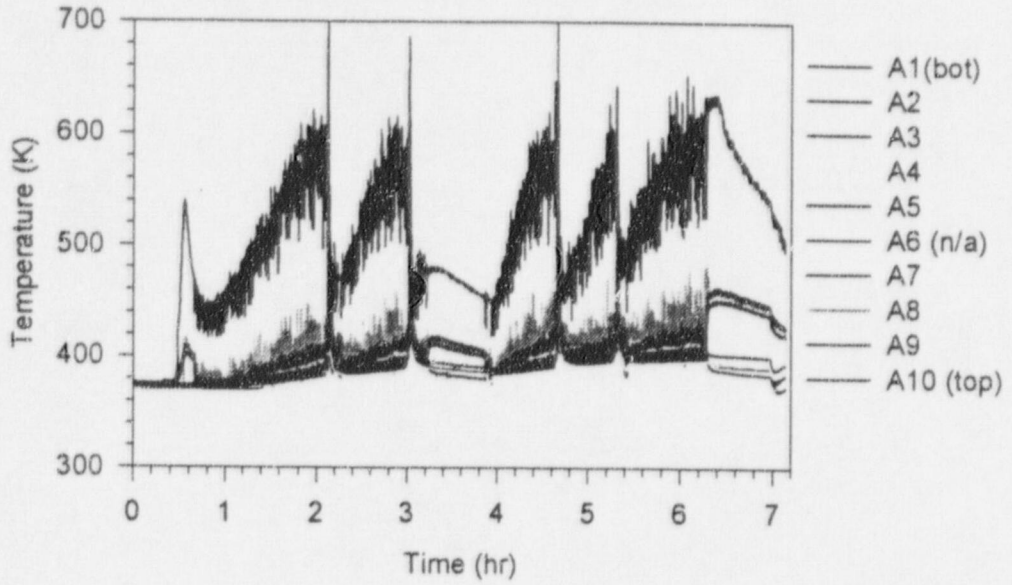

Figure 1. Surtsey vessel centerline gas temperatures from TC array A in PP-2.

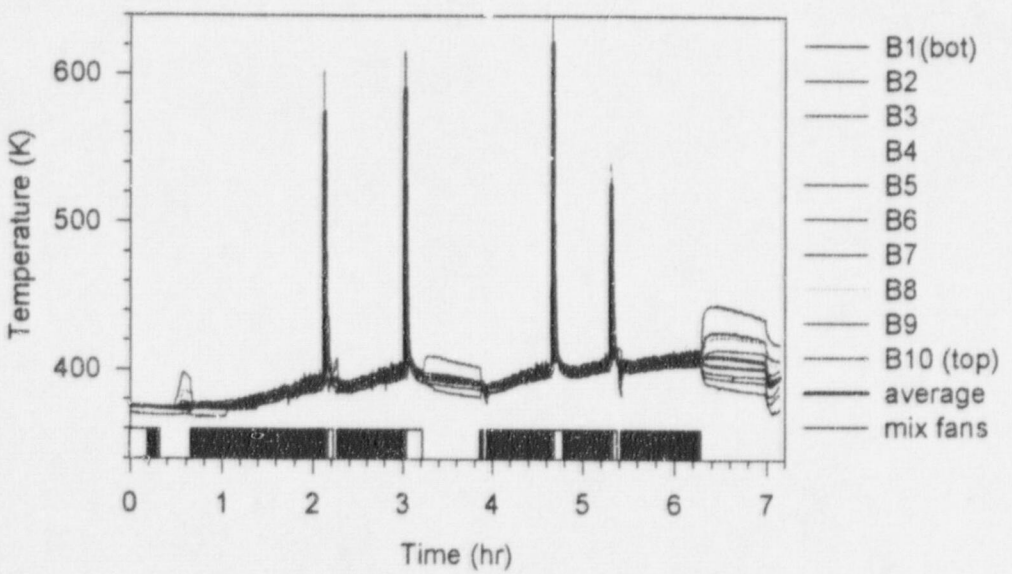

Figure 2. Surtsey vessel wall gas temperatures from TC array B in PP-2.

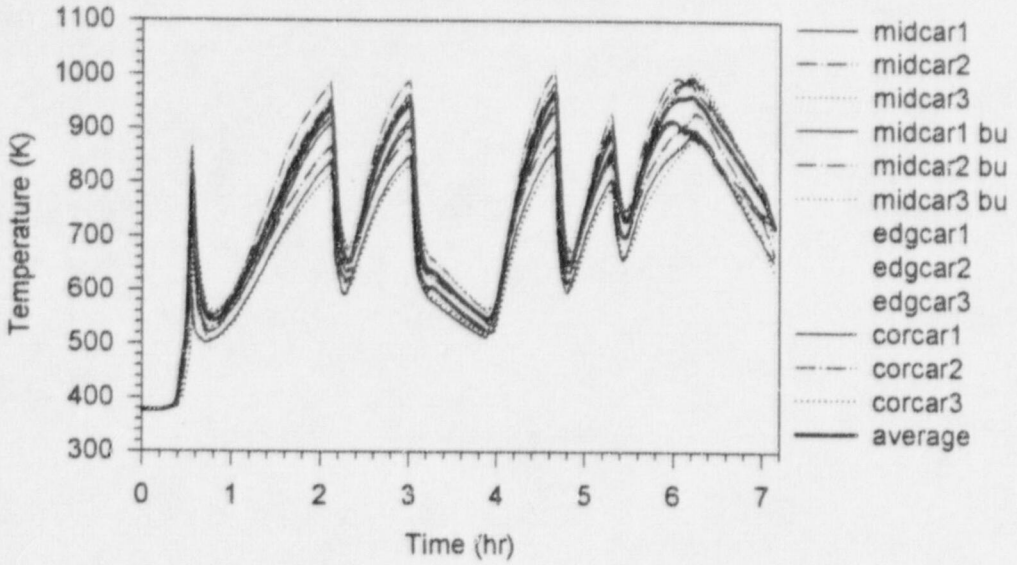

Figure 3. Catalyst cartridge temperatures in PP-2.

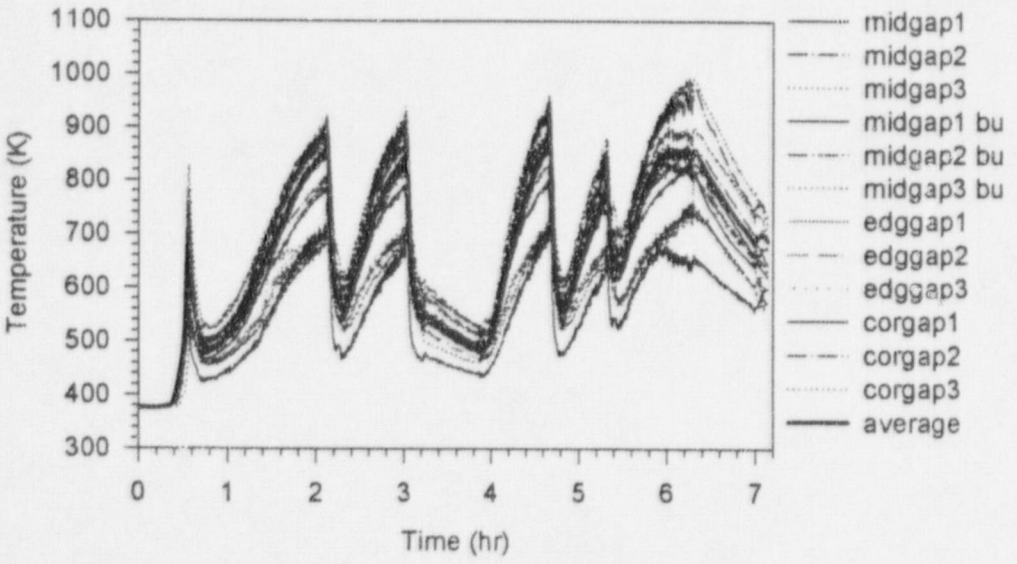

Figure 4. Catalyst gap temperatures in PP-2.

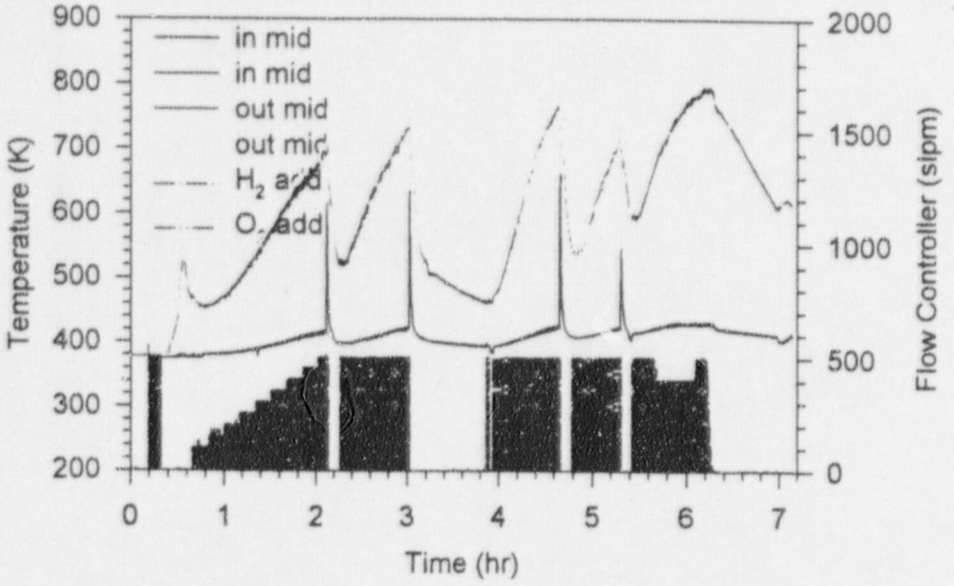

Figure 5. Inlet and outlet temperatures in PP-2.

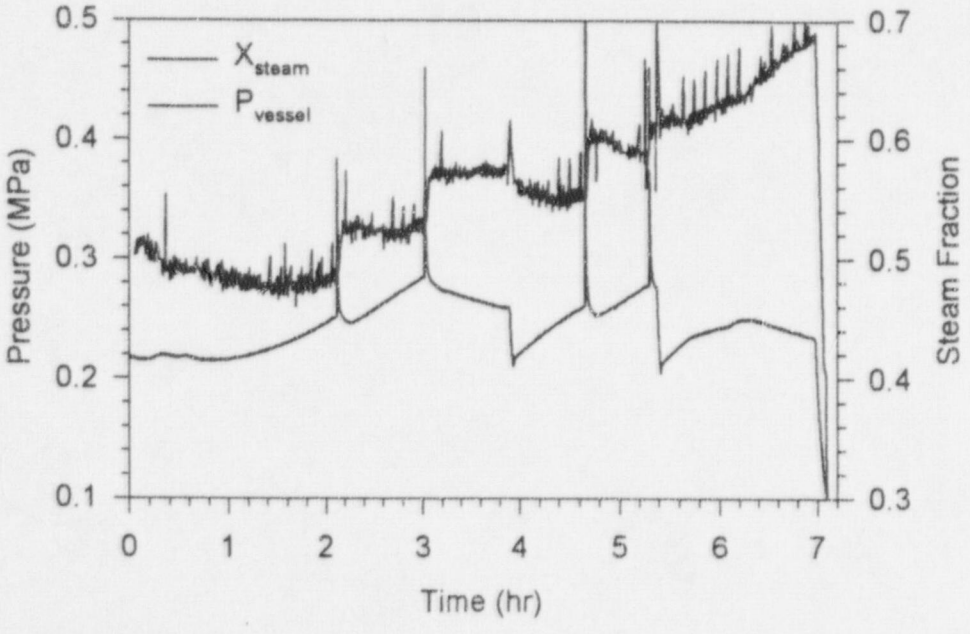

Figure 6. Vessel pressure and steam fraction in PP-2.

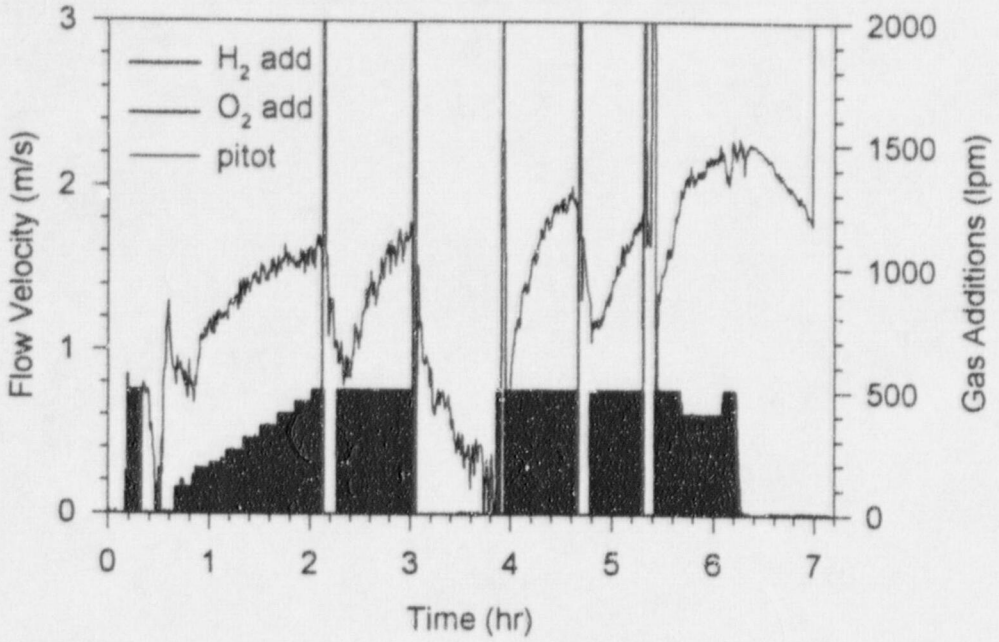

Figure 7. PAR gas velocity in PP-2.

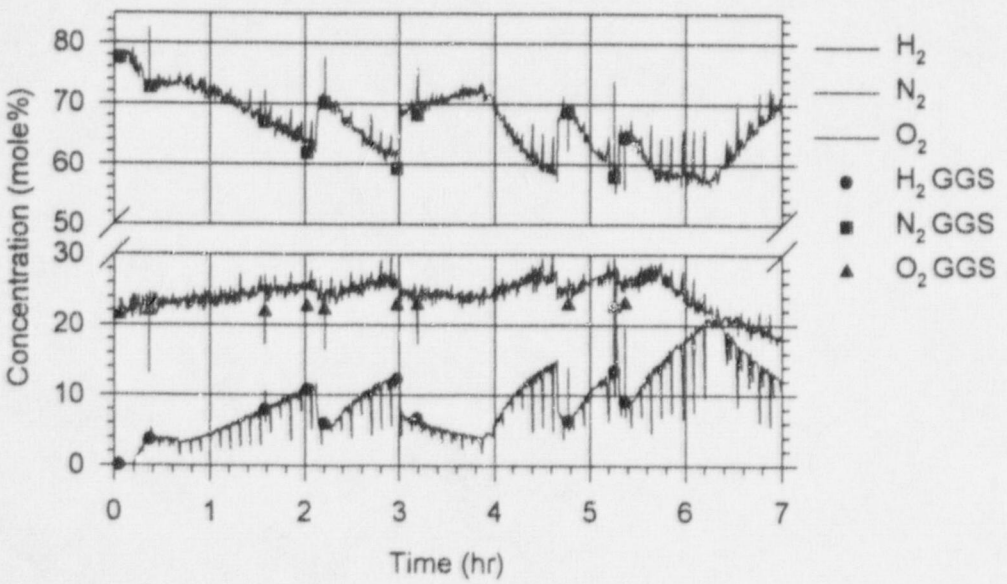

Figure 8. Gas concentrations (dry-basis) in PP-2.

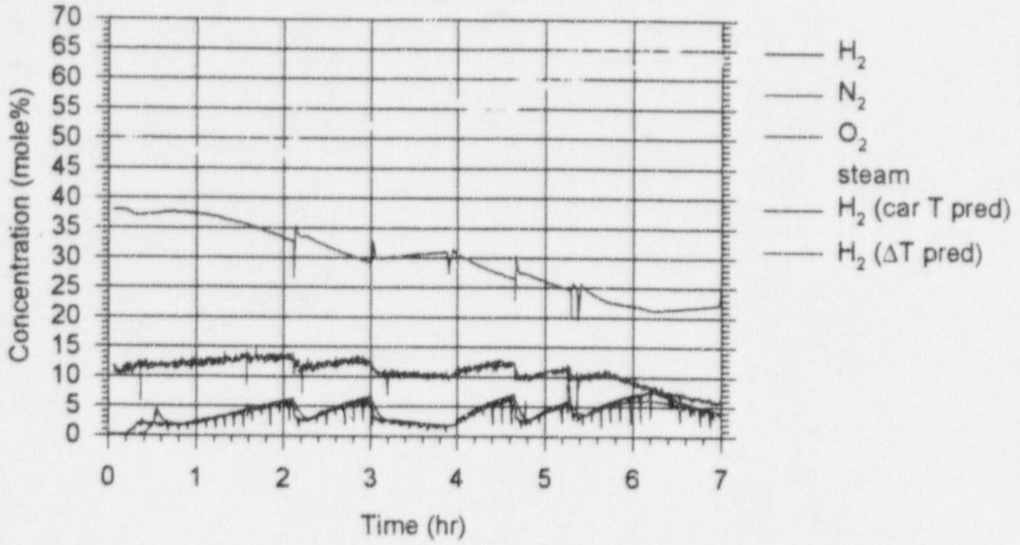

Figure 9. Gas concentrations (wet-basis) in PP-2.

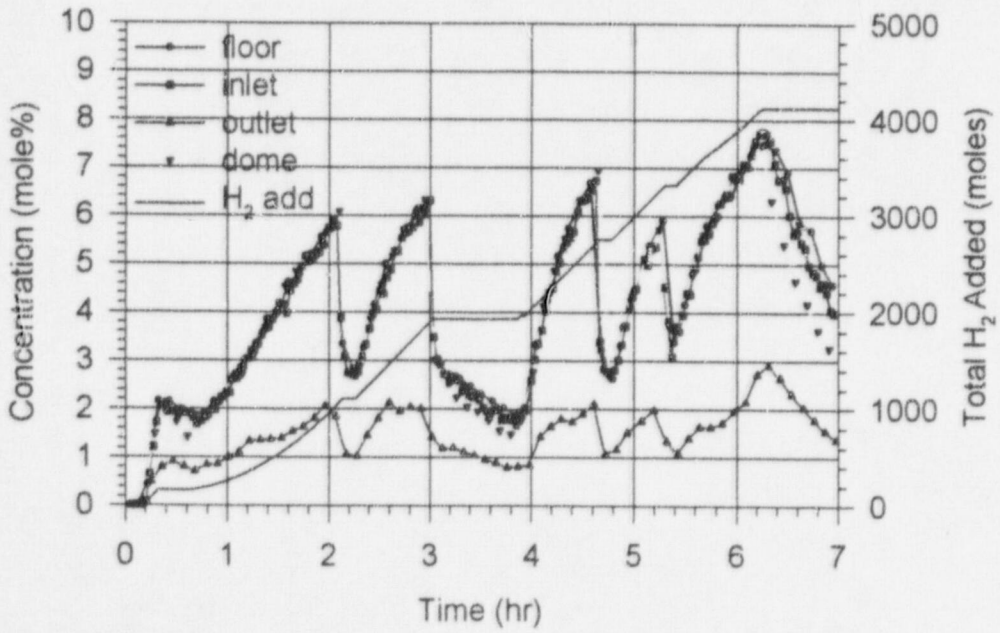

Figure 10. H_2 concentrations (wet-basis) in PP-2.

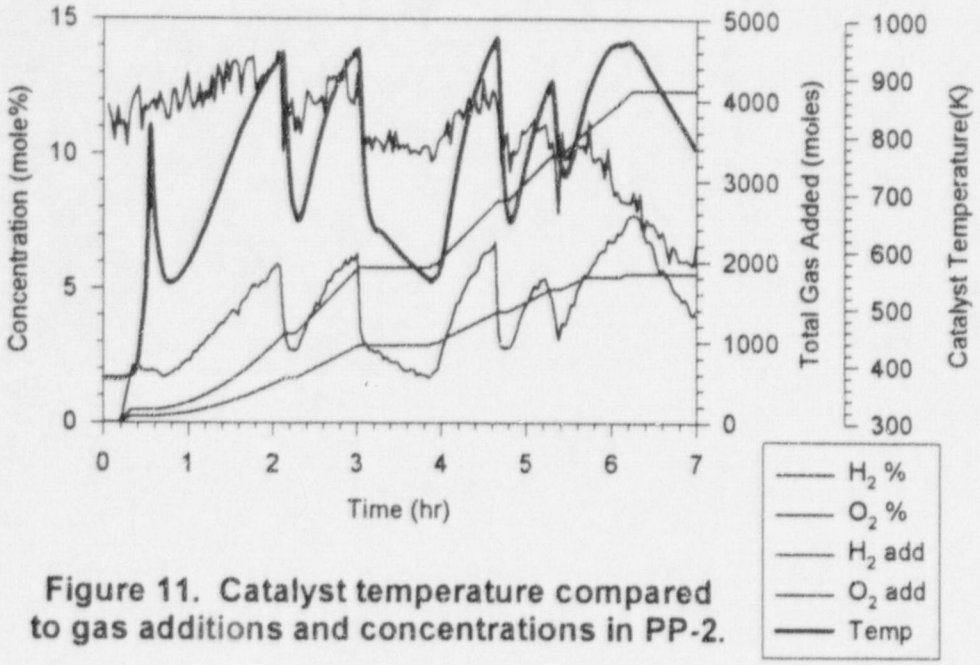

Figure 11. Catalyst temperature compared to gas additions and concentrations in PP-2.

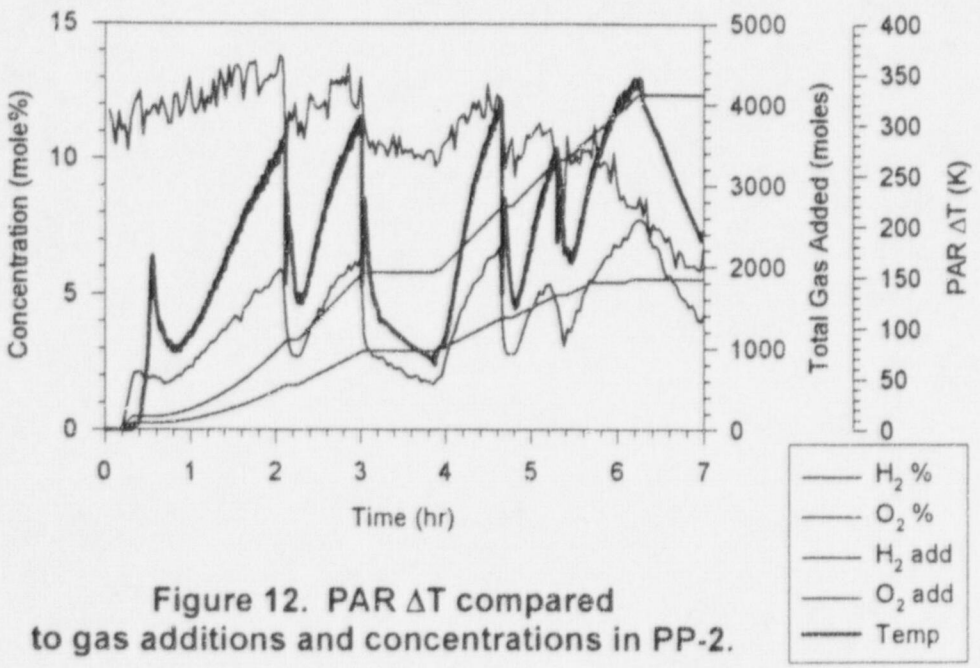

Figure 12. PAR ΔT compared to gas additions and concentrations in PP-2.

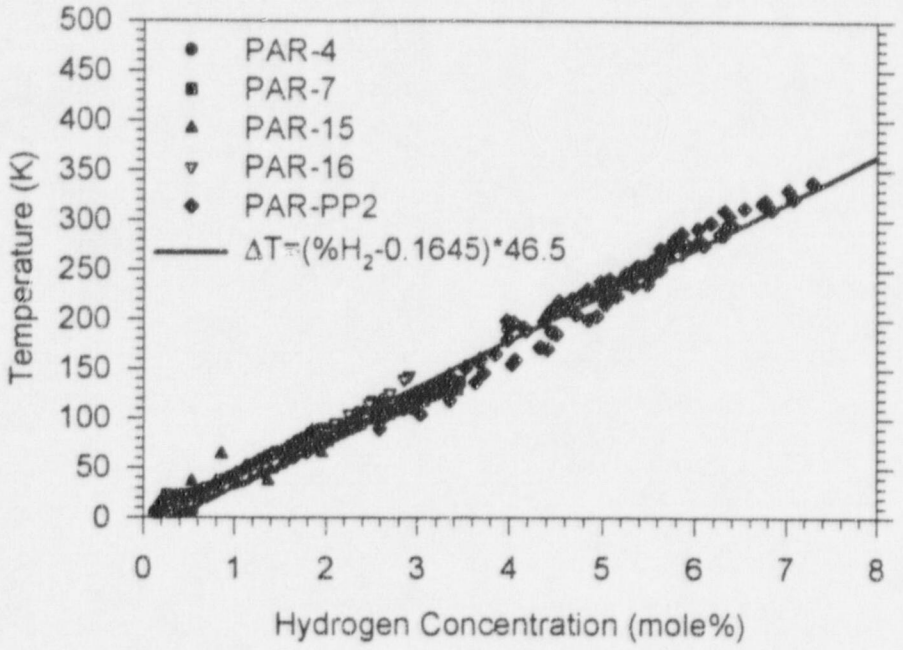

Figure 13. PAR ΔT versus hydrogen concentration.

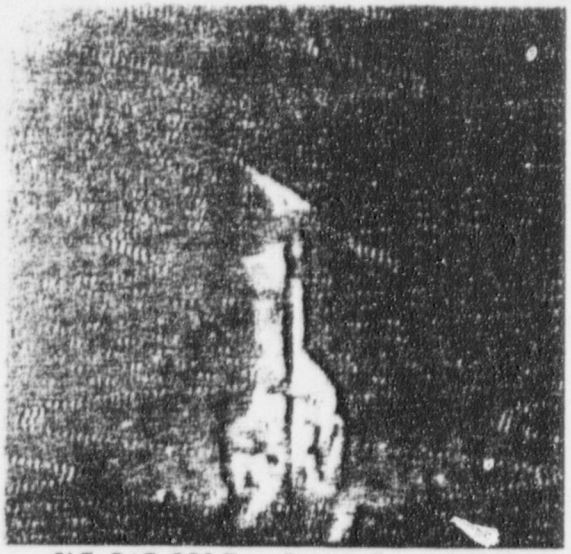

SNL PAR-PP2 Test: Particle Burst (0.00 s)

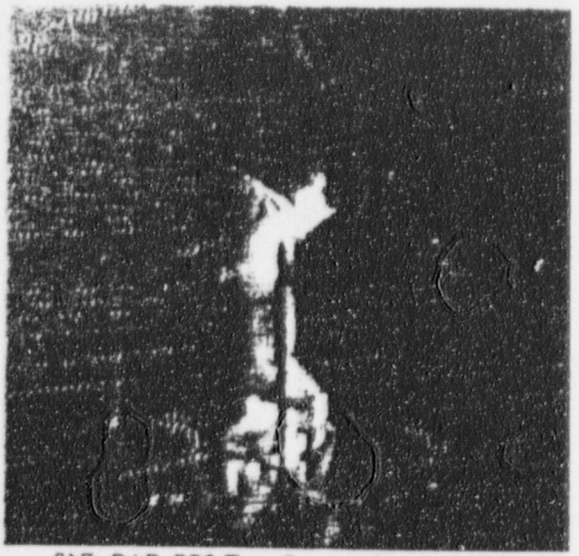

SNL PAR-PP2 Test: Particle Burst (0.50 s)

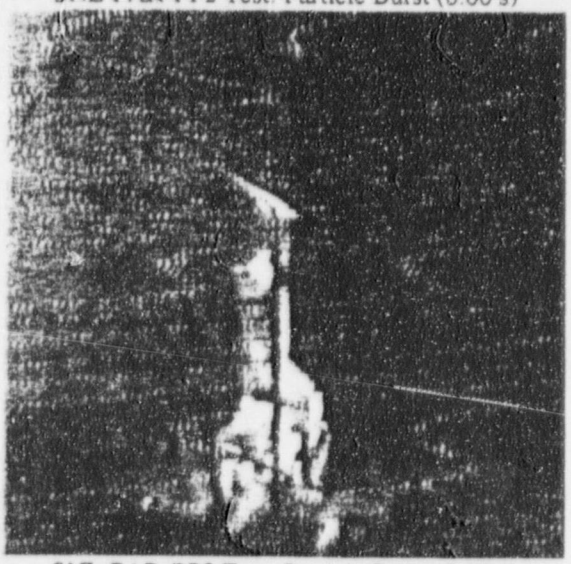

SNL PAR-PP2 Test: Particle Burst (0.17 s)

SNL PAR-PP2 Test: Particle Burst (0.67 s)

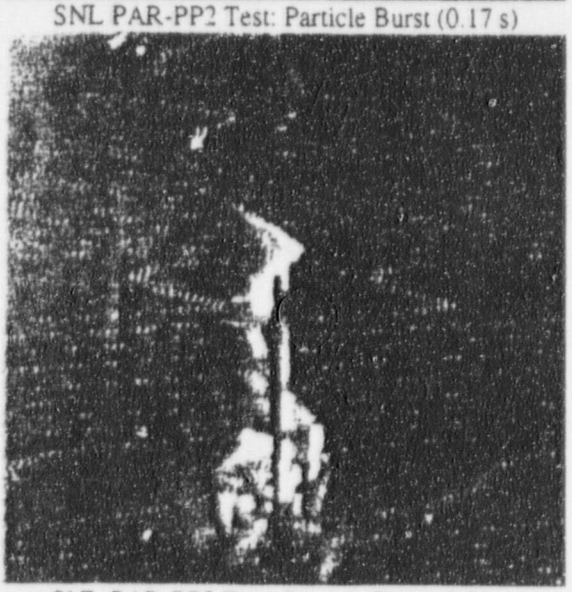

SNL PAR-PP2 Test: Particle Burst (0.33 s)

SNL PAR-PP2 Test: Particle Burst (0.83 s)

SNL PAR-PP2 Test: Particle Burst (1.00 s)

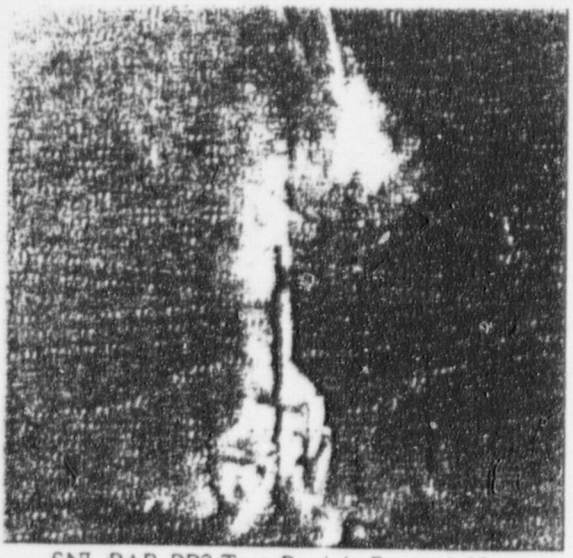

SNL PAR-PP2 Test: Particle Burst (1.50 s)

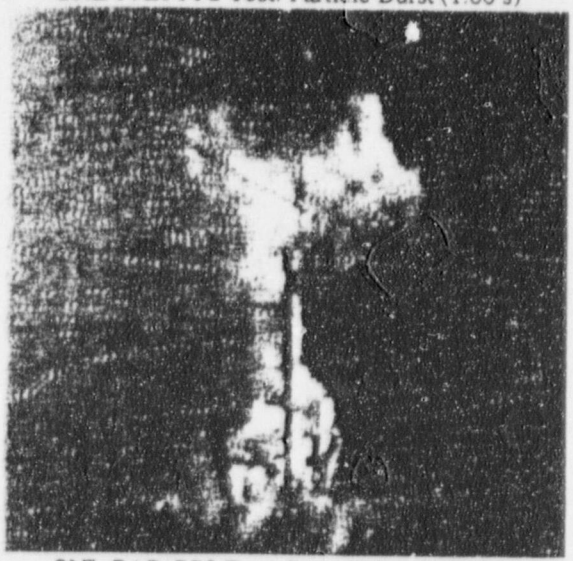

SNL PAR-PP2 Test: Particle Burst (1.17 s)

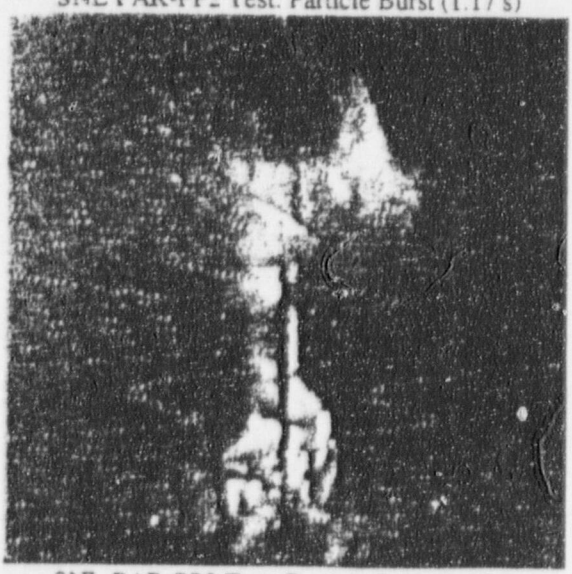

SNL PAR-PP2 Test: Particle Burst (1.33 s)

SNL PAR-PP2 Test: Burn 1 (0.00 s)

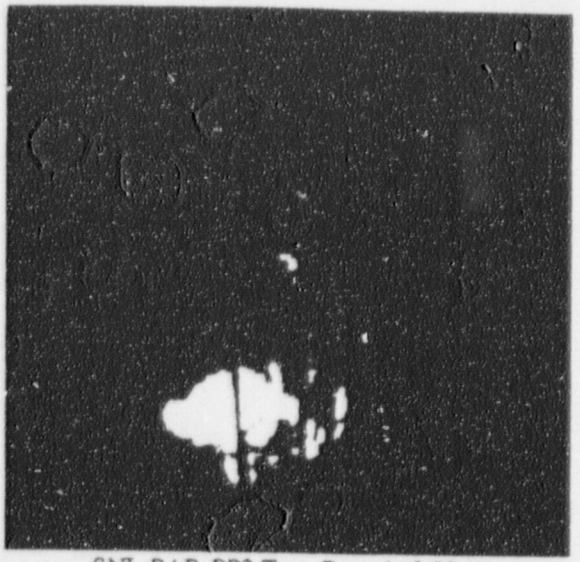

SNL PAR-PP2 Test: Burn 1 (0.50 s)

SNL PAR-PP2 Test: Burn 1 (0.17 s)

SNL PAR-PP2 Test: Burn 1 (0.67 s)

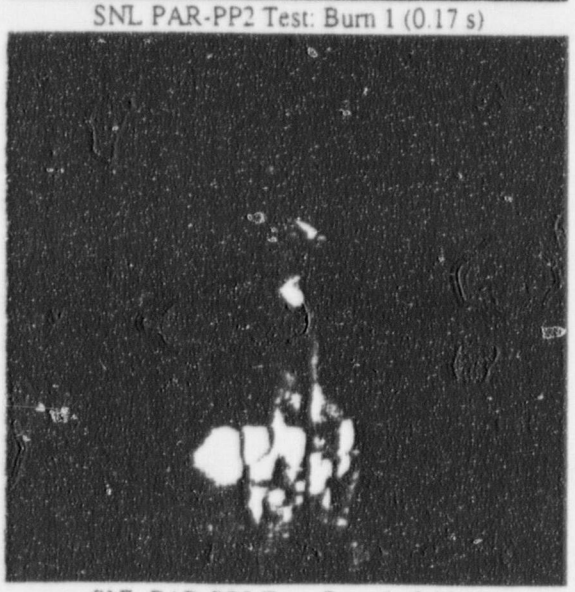

SNL PAR-PP2 Test: Burn 1 (0.33 s)

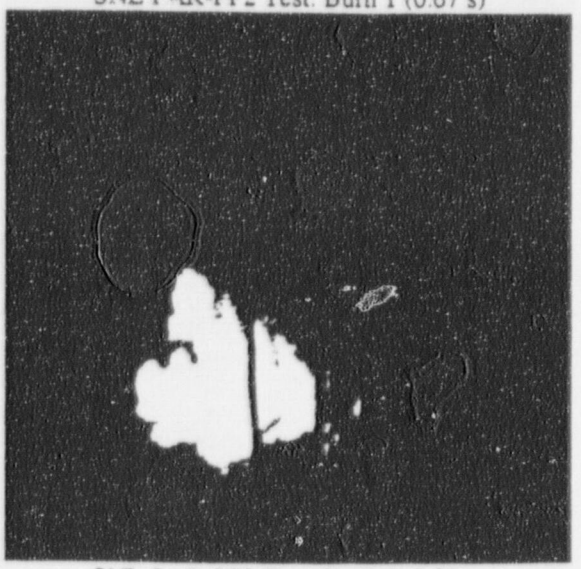

SNL PAR-PP2 Test: Burn 1 (0.83 s)

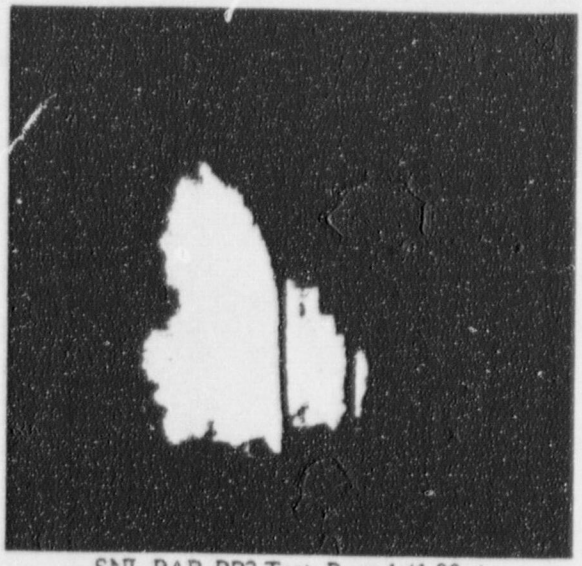

SNL PAR-PP2 Test: Burn 1 (1.00 s)

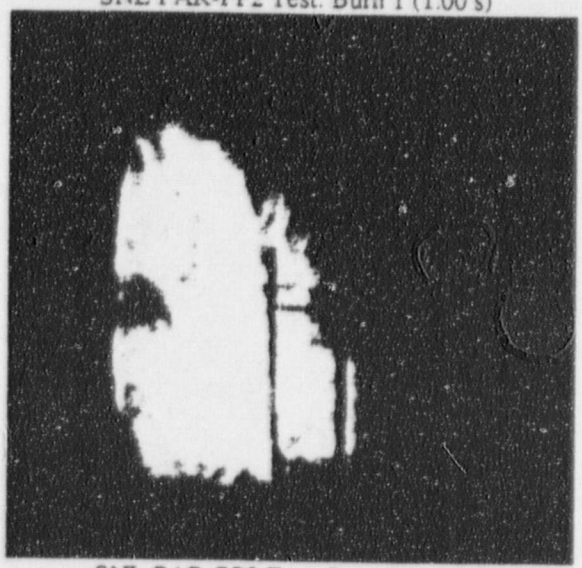

SNL PAR-PP2 Test: Burn 1 (1.17 s)

SNL PAR-PP2 Test: Burn 1 (1.33 s)

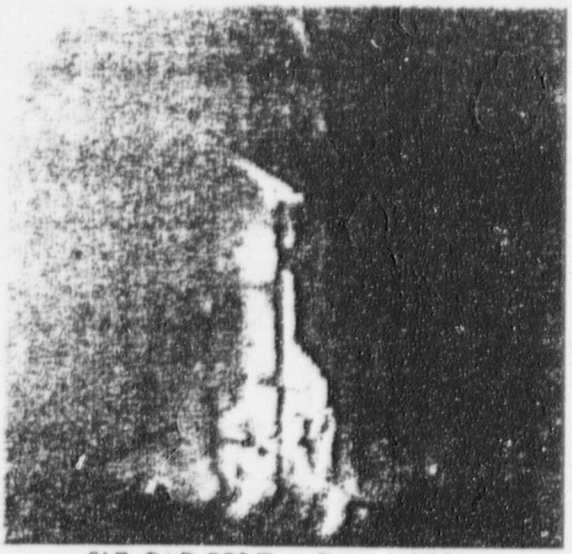

SNL PAR-PP2 Test: Burn 2 (0.00 s)

SNL PAR-PP2 Test: Burn 2 (0.50 s)

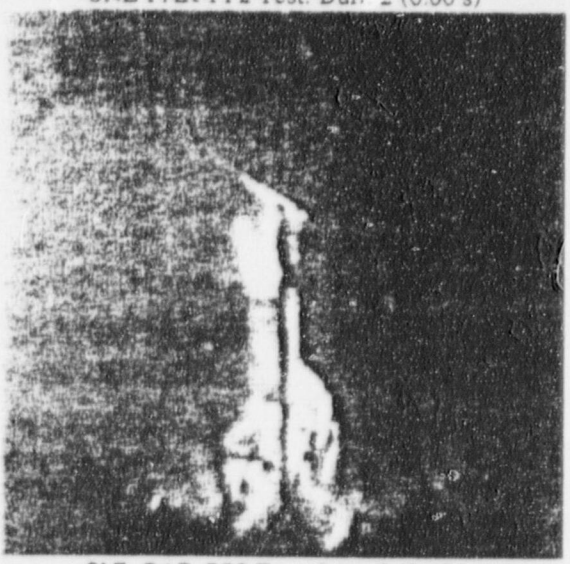

SNL PAR-PP2 Test: Burn 2 (0.17 s)

SNL PAR-PP2 Test: Burn 2 (0.67 s)

SNL PAR-PP2 Test: Burn 2 (0.33 s)

SNL PAR-PP2 Test: Burn 2 (0.83 s)

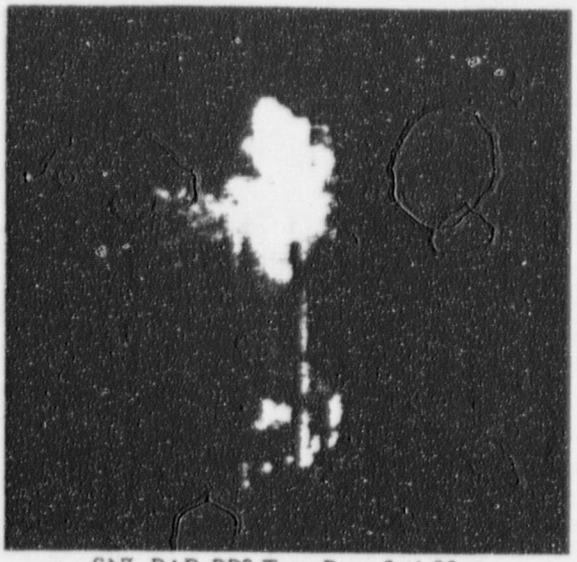

SNL PAR-PP2 Test: Burn 2 (1.00 s)

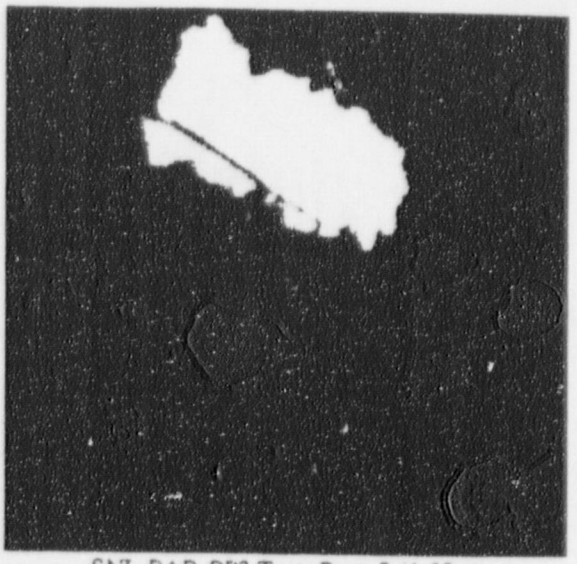

SNL PAR-PP2 Test: Burn 2 (1.50 s)

SNL PAR-PP2 Test: Burn 2 (1.17 s)

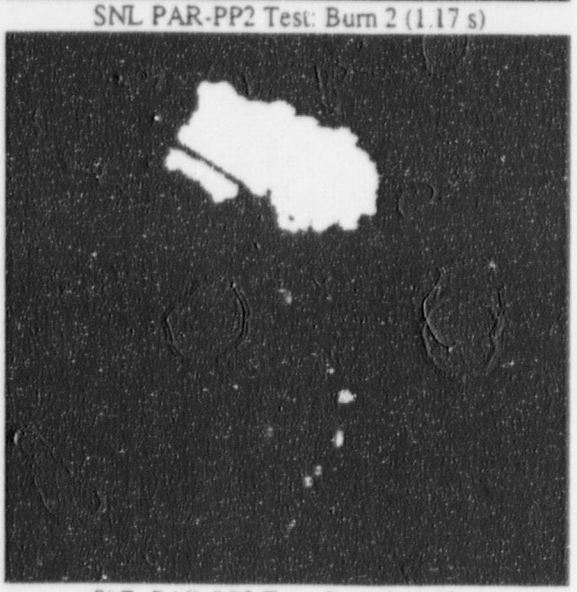

SNL PAR-PP2 Test: Burn 2 (1.33 s)

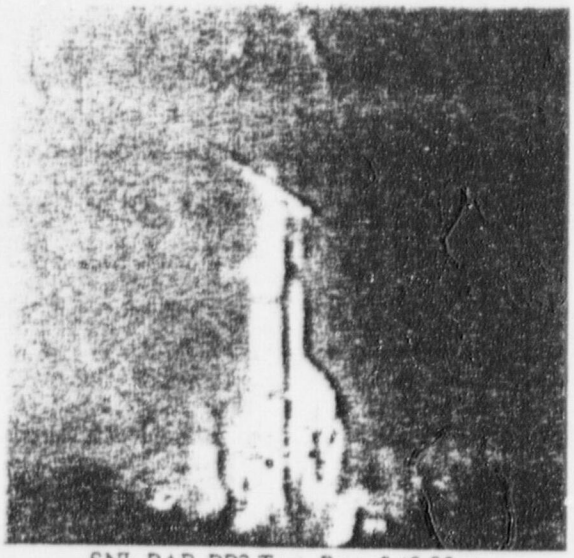

SNL PAR-PP2 Test: Burn 3 (0.00 s)

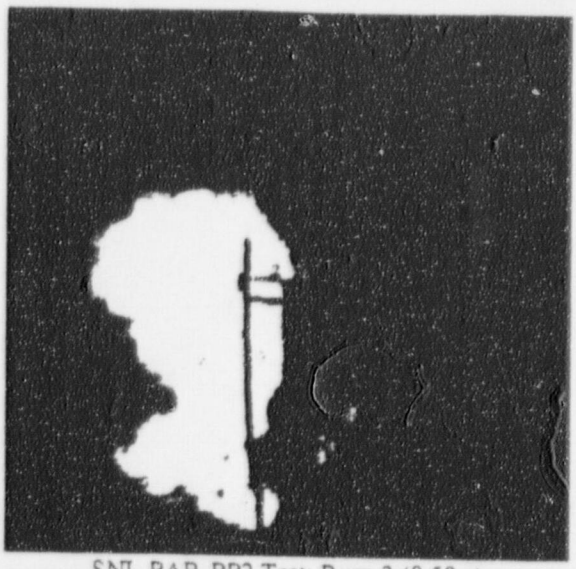

SNL PAR-PP2 Test: Burn 3 (0.50 s)

SNL PAR-PP2 Test: Burn 3 (0.17 s)

SNL PAR-PP2 Test: Burn 3 (0.67 s)

SNL PAR-PP2 Test: Burn 3 (0.33 s)

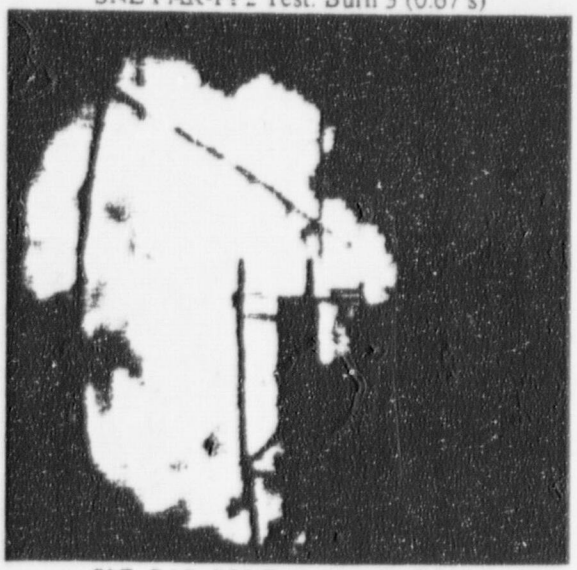

SNL PAR-PP2 Test: Burn 3 (0.83 s)

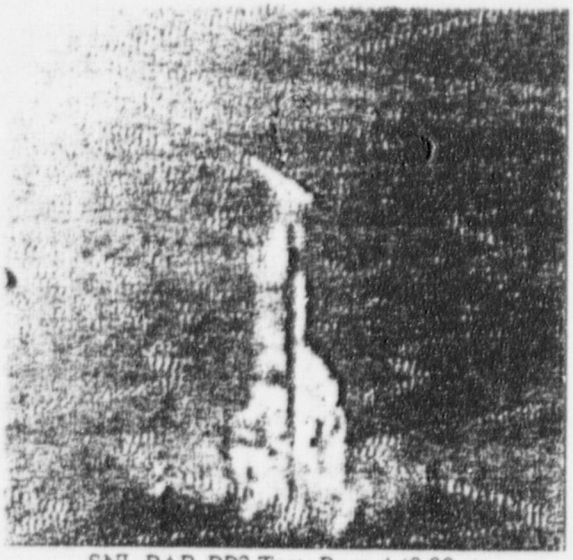

SNL PAR-PP2 Test: Burn 4 (0.00 s)

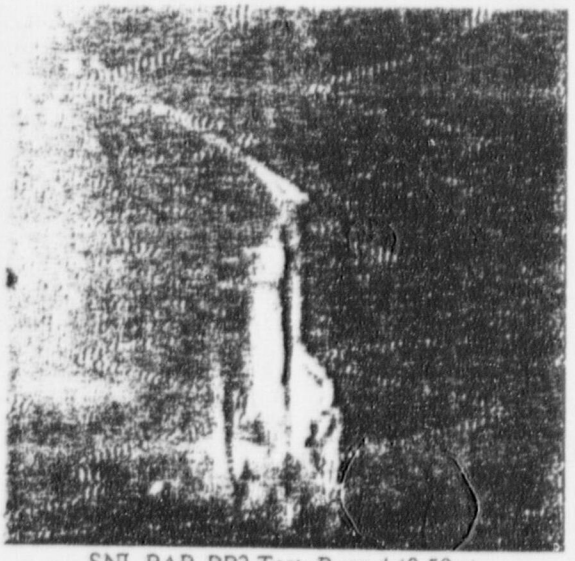

SNL PAR-PP2 Test: Burn 4 (0.50 s)

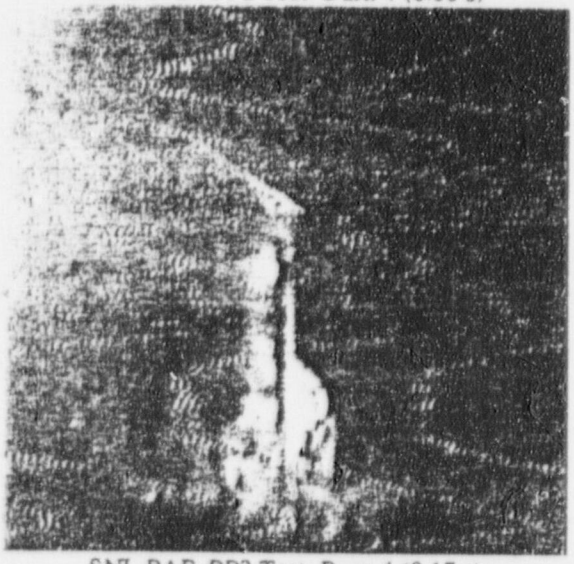

SNL PAR-PP2 Test: Burn 4 (0.17 s)

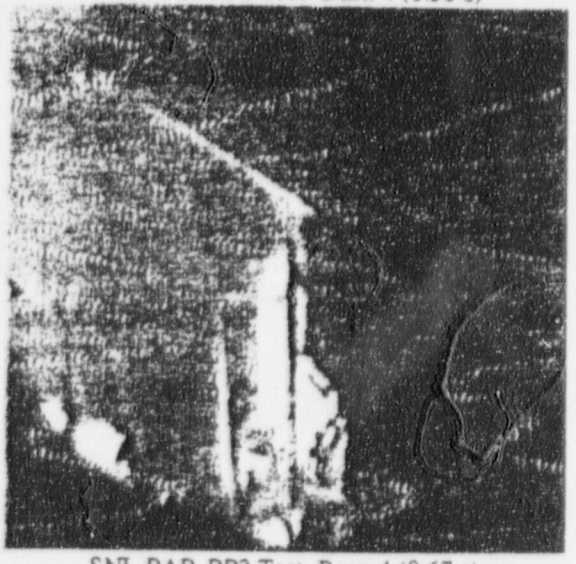

SNL PAR-PP2 Test: Burn 4 (0.67 s)

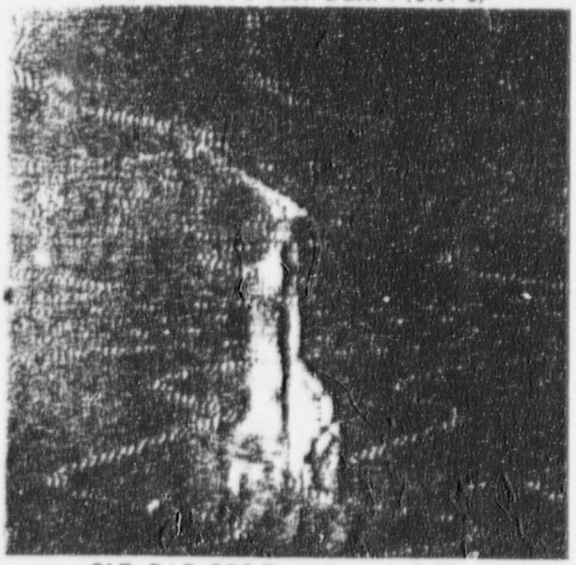

SNL PAR-PP2 Test: Burn 4 (0.33 s)

SNL PAR-PP2 Test: Burn 4 (0.83 s)

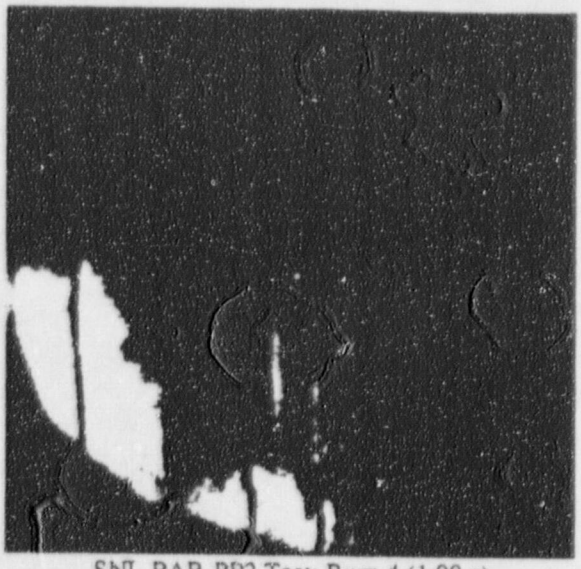

SNL PAR-PP2 Test: Burn 4 (1.00 s)

SNL PAR-PP2 Test: Burn 4 (1.17 s)